

Interannual variability of temperature in the UTLS region upper tropospheric and lower stratospheric (UTLS) region over Ganges-Brahmaputra-Meghna basin based on COSMIC GNSS RO data

Khandu ^a, Joseph Awange^{a,b,c}, and Ehsan Forootan^d

^aDepart of Spatial Sciences, Curtin University, Perth, Australia

^bGeodetic Institute, Karlsruhe University of Technology (KIT), Karlsruhe, Germany

^cDepartment of Geophysics, Kyoto University, Kyoto Japan

^dInstitute of Geodesy and Geoinformation, Bonn University, Bonn, Germany

Correspondence to: Khandu (khandu@postgrad.curtin.edu.au)

Abstract. Poor reliability of radiosonde ~~records~~ ~~observational networks~~ across South Asia imposes serious challenges in understanding ~~climate variability and thermodynamic~~ the structure of the upper-tropospheric and lower-stratospheric (UTLS) region. The Constellation Observing System for Meteorology, Ionosphere, and Climate (COSMIC) mission launched in April 2006 have overcome many observational limitations that are inherent in conventional atmospheric sounding instruments. We examined interannual variability of **UTLS temperature** over Ganges-Brahmaputra-Meghna (GBM) basin **in South Asia** using monthly accumulated COSMIC radio occultation (RO) data, together with two global reanalysis products. Comparisons between August 2006 and December 2013 indicated that MERRA (Modern-Era Retrospective Analysis for Research Application) and ERA-Interim (European Centre for Medium-Range Weather Forecasts reanalysis) were warmer by 2°C between 200 hPa and 50 hPa but these warm bias was found to be consistent over time resulting in a relative bias of $\pm 0.5^\circ\text{C}$. The UTLS temperature showed considerable interannual variability from 2006-2013 in addition to warming (cooling) trends in the troposphere (stratosphere). The cold (warm) anomalies in the upper troposphere (tropopause region) was associated with warm ENSO (El Niño Southern Oscillation) phase while stratospheric sudden warming (SSW) signals were seen in stratospheric temperature anomalies. The tropopause also indicated considerable seasonal variability with its height reaching as high as 18.5 km during the peak monsoon period. PCA (Principal Component Analysis) decomposition of tropopause temperatures and heights over the basin showed ENSO accounts for 73% of the interannual variability with a correlation of 0.77 with Niño3.4 index whereas the quasi-biennial oscillation (QBO) explains about 10% of the variability. The largest tropopause anomaly associated with ENSO occurred during winter, when ENSO was at its peak. The

largest anomaly was recorded during the last major El Niño event of 2009/2010, where tropopause temperature (height) increased (decreased) by about 1.5°C (300 meters). In general, we observed a decreasing (increasing) trend in tropopause temperature (height) during the last 8 years.

Detailed comparisons were also made with various different radiosonde types and Numerical Weather Prediction (NWP) products. The results indicated that Indian Meteorological Department (IMD) radiosondes performed poorly despite upgrading to newer techniques. ShangE (of China) sonde showed the best agreement with COSMIC RO data with a mean temperature difference of -0.06°C and a standard deviation of 1.44°C while the older version (ShangM) indicated a cold bias of 0.61°C in the UTLS region. The inter-annual variability of temperature in the UTLS region based on COSMIC RO data indicated a clear pattern of El Niño Southern Oscillation (ENSO) and Indian Ocean Dipole (IOD) while the stratospheric temperature anomalies reflected all three major Sudden Stratospheric Warming (SSW) events since 2007. The mean tropopause temperature varied from -70°C to -80°C, with an average height of about 15.5 km to 16.3 km from winter to summer, indicating a pronounced annual cycle. The annual amplitudes of tropopause were found to be in the order of 0.6°C and 0.15 km from tropical south to subtropical north. The anomalies of tropopause temperature and height exhibited the patterns of ENSO and IOD exceptionally well with a correlation of 0.65 and -0.52, respectively. The temperature data from Modern Era Retrospective Analysis for Research Application (MERRA) agreed very well with COSMIC RO data.

1 Introduction

The upper troposphere lower stratosphere (UTLS) region (400 hPa - 30 hPa) is characterised by step changes in static stability (temperature lapse rate) with large gradients in a number of radiatively active trace gases, including ozone and water vapour (Reid and Gage, 1985; Randel et al., 2000). The variability and changes in temperature the vertical structure of the UTLS region plays an important role in regulating the exchange of water vapour, ozone, and other trace gases between the troposphere and the stratosphere, which is important for the dynamical and radiative balance of the atmosphere. Observational evidences from balloon-borne radiosondes (1950 onwards) and satellite-based measurements (1979 onwards) suggest that the troposphere has warmed considerably over the past decades with substantial cooling in the lower stratosphere (Karl et al., 2006; Bindoff et al., 2013; Lott et al., 2013; Thorne et al., 2013). Much of this temperature changes has been attributed to the anthropogenic emissions of the well-mixed greenhouse gases, which are consistent with trends from climate model simulations (e.g., Lott et al., 2013; Santer et al., 2008). provides key insights into the underlying causes of global and regional aspects of climate change and is closely associated with the surface temperature fluctuations. The tropopause, which marks the separation between the two boundary layers in the UTLS region is of special importance for understanding the transport of water vapour into the stratosphere and exchange of ozone between the two layers (Randel et al., 2000). On

the other hand, the height of the tropopause is affected by the heat balance of both the troposphere and the stratosphere. For instance, warming of the troposphere due to increasing green house gas concentrations raises the tropopause. Thus, changes in the height of the tropopause provide a sensitive indicator of climate change including human effects on climate, and is a key indicator of global climate change (Santer et al., 2003a, b, 2008). due to its role in tropospheric-stratospheric-exchange process. Observational evidences from balloon-borne radiosondes since the late 1950s and satellite-based measurements since 1979 suggest that the troposphere has warmed considerably over the past decades with substantial cooling in the lower stratosphere. Much of this temperature changes has been attributed to the anthropogenic emissions of the well-mixed greenhouse gases.

While there is are increasing evidences in the recent changes amplification of global and regional in the vertical structure of the UTLS region troposphere and the lower stratosphere including warming (cooling) troposphere (stratosphere) and ozone depletion (see, e.g., Bindoff et al., 2013; Lott et al., 2013), large observational uncertainties still exists in radiosonde measurements over the South Asian continent (specifically over India), which has been highlighted over the years (e.g., Das Gupta et al., 2005; Sun et al., 2010; Kumar et al., 2011; Ansari et al., 2015). especially in the UTLS region due to limited observations. Previous studies have reported anomalously large warm biases in radiosonde observations over India and some stations have been recently updated by the Indian Meteorological Department (IMD) with Global Positioning System (GPS)-based radiosondes to improve their observational skills (see, Kumar et al., 2011). Ansari et al. (2015) reported that GPS-based radiosonde temperature data have improved by many-fold from a bias of 2.6-5.0°C to -0.1-0.1°C. However, our analysis based on 18 radiosondes (15 conventional and 3 GPS-based sondes) over India from August 2006 to December 2013 showed that GPS-based radiosondes still exhibited large warm biases against the COSMIC RO data and anomalously high variations in the UTLS region. The biases were however found to be reduced by more than half from 2.72°C to 1.20°C. As a result, trends in upper air temperatures might be of limited quality, thus, affecting the climate change attribution studies over the region (Seidel et al., 2011; Steiner et al., 2011). Radiosondes can hardly reach up to 50 hPa (~20.5 km) as most of them tend to burst out in the upper tropospheric region. Other issues include instrumental changes over time and poor spatial coverage. Satellite-based Microwave Sounding Units (MSUs) used to retrieve atmospheric information in the UTLS region do not provide adequate vertical resolution and therefore, might indicate systematic biases. For example, previous studies reported anomalously large warm biases in radiosonde observations in the South Asian region, particularly over India.

In order to improve on these limitations, a more robust space-based technique known as the *Global Navigation Satellite System (GNSS) radio occultation (RO)* (e.g., Melbourne et al., 1994; Ware et al., 1996; Kursinski et al., 1997; Awange, 2012) has emerged as an important climate monitoring system over the past decade (see e.g., Anthes, 2011, and reference therein). GNSS RO technique utilises the time delay information of the occulted GNSS signals, which passes through the atmosphere and is

received by Low Earth Orbiting (LEO) satellites. The primary **observables** stobservable are GNSS
 95 phase path and signal amplitude, which can be subsequently converted into atmospheric profiles
 (of e.g., refractivity, temperature) using the assumption of spherical geometry of refractivity (e.g.,
 Melbourne et al., 1994; Rocken et al., 1997). Nowadays, the retrieved bending angles can be di-
 rectly applied in climate- and weather-related studies, thereby introducing less uncertainty in the
 observation system (see, e.g., Lewis, 2009; Schmidt et al., 2010). The use of GNSS RO data is ad-
 100 vantageous since it provides 24-hour global coverage, high vertical resolution, and highly accurate
 profiles of the upper-tropospheric/lower-stratospheric (UTLS) region (see., e.g., Sun et al., 2010;
 Khandu et al., 2011). **Several studies have demonstrated the usefulness of GNSS RO in improving
 numerical weather prediction (NWP) forecasts (e.g., Healy and Thépaut, 2006; Cucurull et al., 2007;
 Poli et al., 2008, 2010), climate studies (Foelsche et al., 2008; Schmidt et al., 2010; Steiner et al.,
 105 2013) and space weather/ionospheric research and operations (e.g., Lee et al., 2012; Zhang et al.,
 2014) over the past two decades.** The number of RO profiles ~~have~~ **has** increased substantially over
 the past years with the launch of several GNSS RO missions enabling wider applications in regional
 studies (see, e.g., Anthes, 2011). For instance, the joint Taiwan-US mission Constellation Observ-
 ing System for Meteorology, Ionosphere, and Climate (COSMIC)/FORMOSA Satellite Mission 3
 110 (COSMIC/FORMOSAT-3, hereafter, COSMIC) (Anthes et al., 2008) has recorded about 1500 RO
 soundings per day globally with 70-90% of the soundings reaching within one km of the Earth's
 surface **since August 2006.**

**Several studies have analyzed the long-term variations of temperature in the UTLS region such
 as annual, monthly, seasonal, and interannual variations using observations from global network of
 115 radiosondes, satellite-based measurements, and global reanalysis including the various aspects of
 tropopause characteristics (e.g., Reid and Gage, 1985; Randel et al., 2000; Gettelman et al., 2001;
 Gettelman and de F. Foster, 2002; Santer et al., 2003a, b; Seidel and Randel, 2006; Wilcox et al.,
 2011; Lott et al., 2013). Large-scale temporal variability of the tropopause is dominated by an annual
 cycle and longer-term interannual variability associated with large-scale ocean-atmospheric circula-
 120 tion phenomenon such as El Nino Southern Oscillation (ENSO, Trenberth, 1990) and stratospheric
 zonal wind variations, also known as quasi-biennial oscillation (QBO, Baldwin et al., 2001). The
 ENSO mode is depicted as a dumbbell pattern in the central Pacific (Randel et al., 2000; Gettelman
 et al., 2001) while QBO mode is a symmetrical structure across the equator (Randel et al., 2000).
 Over the Indian monsoon region, Kulkarni and Verma (1993) found that the composites of mean
 125 tropopause height was significantly higher for good monsoon years, which coincides with the cold
 ENSO events. With the increasing record of GNSS RO record both in time and space, it is now
 possible to infer decadal temperature trends in the UTLS region and the tropopause with a struc-
 tural uncertainty of less than 0.06°C in the tropics and mid-latitudes (Steiner et al., 2013). Based
 on the approximately 9 years of GNSS RO data from CHALLENGING Minisatellite Payload (CHAMP,
 130 2001-2008 Wickert et al., 2001), Gravity Recovery And Climate Experiment (GRACE, 2006-2009**

Wickert et al., 2009) and COSMIC (2006-2009), Schmidt et al. (2010) found an increase of global tropopause height (5-9 m/year) with an upper tropospheric warming and a lower stratospheric cooling. In general, the tropopause height variations are positively (negatively) correlated with upper tropospheric (lower stratospheric) temperature variations.

135 While many studies have been conducted to re-assess the global as well as regional lower atmospheric structure using the RO profiles, including their accuracies, only few such assessments have been carried out over the Indian sub-continent.

From the hydrological perspective, the Ganges-Brahmaputra-Meghna (GBM) river basin in South Asia is a complex region consisting of the Himalayas (in the north) and vast alluvial flood plains (in the south) and also consists of the world's third largest freshwater outlet (Chowdhury and Ward, 2004). The highly seasonal southwest Indian monsoon lasts from June to September with the rest of the period remaining relatively dry. While short-term variations in monsoon are associated with deep convective activities and horizontal advection through cold trap regions, modulation by equatorial planetary waves (e.g., Mehta et al., 2010), long-term variations are modulated by ENSO and the Indian Ocean Dipole (IOD, Saji et al., 1999) mode, another large-scale coupled ocean and atmosphere phenomenon in equatorial Indian ocean. The two modes (ENSO and IOD) generally have opposite effects over the region in terms of the precipitation with lower than normal rainfall during warm ENSO phase (also called El Niño) and higher than normal rainfall during positive IOD events (e.g., Ashok and Saji, 2007; Krishnamurti et al., 2013). The surface air temperature was found to be warmer in summer during El Niño events while winter and spring surface temperatures were found to be mainly induced by Indian Ocean sea surface temperature (SST) anomalies (Chowdary et al., 2014). Although relatively new, it is likely that IOD mode may have a significant impact on the variability of temperature in the UTLS region due to their significance on the regional atmospheric process. offers an interesting view on the regional perspective of the variability of UTLS because of its hydrological importance and intense activity of Indian monsoon from June to September. Previous studies have suggested that tropopause heights could be used as an additional indicator of Indian monsoon due to its high correlation with rainfall in May (Kulkarni and Verma, 1993). The rising mountains along the southern foothills of the Himalayas act as barriers to the Indian monsoon generating deep convection along the Himalayan fronts, which may affect the spatial variability of tropopause parameters such as temperatures and heights. The growing population and expanding industrialisation in and around the GBM basin are the major source of atmospheric pollution and greenhouse gases (GHGs), and a key modulator of the UTLS region including the tropopause (Gautam et al., 2009; Lau et al., 2009). Thus, long-term self-calibrated GNSS RO data from various RO missions will help to provide valuable information on the regional climate change in future as indicated by several studies (see, e.g., Schmidt et al., 2008; Steiner et al., 2011, 2013).

The objective of this study is to examine interannual variability of temperature in the UTLS region over the GBM basin using approximately 8 years of monthly accumulated RO data from the

COSMIC mission (August 2006- December 2013), together with global reanalysis fields from European Centre for Medium-Range Weather Forecasts reanalysis (ERA-Interim, Dee et al., 2011) and Modern-Era Retrospective Analysis for Research Application (MERRA, Rienecker et al., 2011). Reanalysis products have proven to be very useful in understanding the thermodynamics of the lower atmosphere as well as the tropospheric-stratospheric exchange process by assimilating observations from various platforms including radiosondes, wind profilers, air crafts, and satellites measurements (Poli et al., 2010; Dee et al., 2011; Rienecker et al., 2011). While the primary goal for ERA-Interim has been to address several difficult data assimilation problems in ERA-40 mainly relating to the representation of the hydrological cycle, the quality of the stratospheric circulation, and the consistency in time of reanalysed geophysical fields (Dee et al., 2011), MERRA was developed primarily to improve on various aspects of the hydrologic cycle that were not adequately represented in previous generations of reanalyses (Rienecker et al., 2011). ERA-Interim also assimilates refractivity profiles retrieved from GNSS RO missions from 2001 to reduce temperature biases with respect to radiosondes in the ERA-Interim background (Poli et al., 2010; Dee et al., 2011). Thus, modern reanalysis such as MERRA and ERA-Interim are expected to accurately capture the interannual variabilities of temperature in the UTLS region for the most recent decade. This study investigates the interannual variability of temperature in the UTLS region and tropopause parameters (temperatures and heights) over the GBM basin for the period August 2006 to December 2013 (89 months) using the GNSS RO profiles from the COSMIC RO mission. Further, COSMIC RO data are compared with Modern-Era Retrospective Analysis for Research Application to assess the interannual variability of temperature of the UTLS region. It should be pointed out that no specific study involving MERRA products have been carried over the region. Three specific objectives are outlined as follows; (i) intercompare COSMIC RO retrieved profiles with radiosonde observations and reanalyses products, with specific focus on the upgraded radiosondes over India, (ii) analyse the interannual variability of UTLS temperature (400-30 hPa or 7.5-24.0 km), and (iii) assess the interannual variability of tropopause over the GBM basin. The use of retrieved parameters such as refractivity, temperature, and water vapour from COSMIC RO data accounts for the overall error budget of the GNSS RO technique.

The remainder of the study is organised as follows. In Section 2, the study region is presented. This is followed in Section 3 by the description of datasets and methods used. ,with the interpolation algorithm used to interpolate the point-based COSMIC RO datasets presented in the Appendix. The results are presented and discussed in Section 4, and Section 5 concludes the study.

2 Ganges-Brahmaputra-Megha Basin

The GBM river basin in South Asia is a combination of three medium to large river basins, namely, Ganges basin (907,000 km²), Brahmaputra basin (583,000 km²) and the Meghna basin (65,000 km²) (Chowdhury and Ward, 2004). This transboundary river basin with an elevation range from

the sea level to more than 8,000 m is shared by 5 countries (India (64%), China (18%), Nepal (9%), Bangladesh (7%) and Bhutan (3%), see, Figure 1). The GBM river basin with a total surface area of approximately 1.75 million km² features distinct climatic characteristics owing to its diverse climate and other factors such as high topographic variations, the Indian Monsoon, and its interaction with large scale circulations (e.g., Chowdhury, 2003). For instance, Ganges basin is generally characterised by low precipitation while Brahmaputra and Meghna basins are characterised by high rainfall amount (Mirza et al., 1998). The Himalayan fronts (e.g., Meghalayan Plateau) act as an immediate barrier to the summer monsoonal flow and are usually characterized by pronounced rainfall along the Himalayan fronts and across the southern foothills (Barros et al., 2004).

[FIGURE 1 AROUND HERE.]

The atmospheric conditions over the basin are largely controlled by the monsoonal circulation during summer (e.g., Kripalani et al., 2007), which is often modulated by global and regional large-scale climate variabilities such as ENSO and IOD (e.g., Chowdhury, 2003; Ashok and Saji, 2007). The impact of global warming and regional climate change arising from increasing population and rapid industrial and agricultural activities, and landuse changes across the basin may have resulted in a warmer troposphere over the years (Gautam et al., 2009; Lau et al., 2009).

3 Data and Methods

3.1 FORMOSAT/COSMIC RO Data

COSMIC Level 2 RO data covering the GBM basin (see, Figure 1) for the period April 2006 to December 2013 was obtained from the COSMIC Data Analysis and Archive Center (CDAAC) at the University Corporation for Atmospheric Research (UCAR). ~~for the period August 2006 to December 2013 was used in this study.~~ CDAAC maintains an archive of RO profiles from all many previous and existing RO missions including FORMOSAT/COSMIC (2006-2015), CHALLENGING Minisatellite Payload (CHAMP, 2001-2008), Gravity Recovery and Climate Experiment (GRACE, 2006-2015), etc. COSMIC is a six-satellite mission launched on the 14th of April 2006, with the goal of using GNSS RO data for various atmospheric and weather-related applications (Anthes et al., 2008). With an average sounding of around 1,500-2,000 profiles per day (at ~100 m to 1 km vertical resolution and ~300 km horizontal resolution), COSMIC has become a highly successful RO mission with high positive impacts especially on the operational weather forecasts (see e.g., Anthes et al., 2008; Ho et al., 2010; Anthes, 2011) and global atmospheric studies (see e.g., Foelsche et al., 2008; Schmidt et al., 2010). The bending angle (α) with an impact parameter values (a) derived from Doppler shift measurements from RO can be inverted with an Abel transform to recover refractive index (n) profiles (or refractivity, $N = 10^6(n - 1)$), which are in fact related to total pressure (P), temperature (T) and water vapour pressure (P_w) as shown in Mel-

bourne et al. (1994). For the dry atmosphere ($P_w=0$) density profiles are obtained from the known relationship between refractivity and density while pressure and temperature (“dry temperature”) can be derived using the hydrostatic equation and equation of state for ideal gas (see, Melbourne et al., 1994). In the presence of water vapour (especially in the lower troposphere), humidity and temperature profiles can be obtained using priori information (or background information) such as numerical weather forecasts. Alternatively, CDAAC also provides a modified refractivity profiles (called “wet profiles”) using the one-dimensional Variational (1D-Var) method that combine information provided by GNSS RO and a given priori information in a statistically optimal way (see, <http://cdaac-www.cosmic.ucar.edu/cdaac/status.html>). The refractivity (N) and temperature (T) profiles retrieved from raw GNSS signals are referred to as the *dry profiles*. The raw refractivity profiles are separately processed using a 1D-Var (one dimensional variational) analysis with background information from numerical weather forecasts to provide accurate estimates of temperature and humidity in the troposphere. These profiles are referred as the *wet profiles* and contains information on refractivity, temperature, and water vapour pressure (or relative humidity). CDAAC uses a coarse grid background data from the European Centre for Medium-Range Weather Forecasts (ECMWF) re-analysis. The wet and dry profiles mainly differ in the lower troposphere due to presence of water vapour but are highly accurate between 8 and 20 km (see, Anthes et al., 2008). The *a priori* information (i.e., ECMWF) is minimally influenced by radiosonde observations in the GBM basin as they were not included in ECMWF (Kummar 2010). In this study, we used both dry and wet profiles of COSMIC RO to examine their differences over the GBM basin.

The GBM basin recorded 59,419 COSMIC received a total of 35,776 profiles from April 2006 to December 2013, out of which $\sim 14\%$ were found to be of bad quality. Figure 2a shows the temporal record of total monthly profiles recorded during the period, averaging to ~ 576 profiles in a month from August 2006 to December 2013. The number of profiles drastically went down between late 2010 and 2012 (Figure 2a) due to increasing number of problems in the individual COSMIC satellites (for details, see, <http://cdaac-www.cosmic.ucar.edu/cdaac/status.html>). at an average of ~ 388 profiles per month (see, Figure 2a). Figure 2b shows the distribution of RO data points at various pressure (altitude) levels indicating that COSMIC data is able to penetrate deep into the lower troposphere with more than 56% of the profiles reaching at least 850 hPa (~ 1.5 km above MSL). Geographical distribution of COSMIC profiles at 850 hPa (~ 1.5 km), 700 hPa (~ 3.1 km), 500 hPa (~ 6.0 km), and 400 hPa (~ 7.5 km) in Figure 3a-d indicates that their locations match very well with the topography of the region (see, Figure 1). shows the spatial distribution of COSMIC RO data at , which indicated generally a good correlation with the surface topography of the basin (Figure 1). A near-complete coverage of the RO data can be seen at 400 hPa (~ 7.5 km), which corresponds corresponding to the altitude of Himalayas.

[FIGURE 2 AROUND HERE.]

[FIGURE 3 AROUND HERE.]

3.2 Reanalysis Products

The temperature profiles of COSMIC RO data over the GBM region were compared with two high-resolution modern reanalysis products, (a) Modern-Era Retrospective Analysis for Research Application (MERRA, Rienecker et al., 2008) and European Centre for Medium-Range Weather Forecasts (ECMWF) retrospective analysis (ERA-Interim, Dee et al., 2011), both of which were developed to address specific problems in the previous reanalysis systems. MERRA is a global re-analysis data produced by the state-of-art Goddard Earth Observing System Data Assimilation System, version 5 (GOES-5) general circulation model (GCM) at National Aeronautic and Space Administration (NASA), US. GEOS-5 assimilates data from a wide variety of observing systems (e.g., *in-situ*, satellites, etc.) , which are integrated forward in time using a finite-volume dynamics to produce a consistent set of spatio-temporal meteorological and climatic variables since the beginning of the satellite-era (i.e., 1979). An improved land-process model known as the *Catchment Land Model* has been integrated into the GCM to improve the global hydrological cycle (Rienecker et al., 2008). GEOS-5 is run at a horizontal resolution of $1/2^\circ \times 2/3^\circ$ (or $\sim 50 \times 70$ km) and has 72 vertical layers extending from the surface through to the stratosphere. Atmospheric variables (e.g., temperature, humidity) are produced at various temporal scales ranging from 3-hourly at $1.5^\circ \times 1.5^\circ$ (or $\sim 150 \times 150$ km spatial resolution), to monthly scales at the nominal horizontal resolution. GEOS-5 uses radiosondes as the predominant source of information in the model atmosphere, which are further augmented by other atmospheric sensors such as dropsondes, pilot balloons, and raw radiance measurements from satellites (e.g., Advanced MSU) that are weighted according to their observational error variances (see, Rienecker et al., 2008, for details).

ERA-Interim is the latest global atmospheric reanalysis produced by the ECMWF covering the period 1979 to present (Dee et al., 2011). ERA-interim builds on the previous generation of re-analyses (such as ERA-15 and ERA-40) at the ECMWF with improved model aspects, more advanced assimilation techniques (e.g., 4D Variational Schemes) and better land surface model, and assimilates the latest atmospheric profiles retrieved from the GNSS RO data. The products simulated by ERA-Interim include a large variety of 3-hourly surface parameters, and 6-hourly upper-air parameters from the surface up to 0.1 hPa (stratosphere), which are reported at 60 vertical levels at $\sim 79 \times 79$ km spatial resolution (or at spectral resolution of T255). Because ERA-Interim uses newly derived radiosone temperature bias adjustment as well as GNSS RO data, the differences between ERA-Interim and COSMIC RO are likely to be biased. Poli et al. (2010) found that GNSS RO data helps to reduce temperature bias at the tropopause and stratosphere but found drying effect in the mean water-vapour content in the tropics in ERA-Interim. Monthly mean temperature at 14 pressure levels from 500 hPa to 10 hPa were obtained from both MERRA (see, <http://disc.sci.gsfc.nasa.gov/daac-bin/FTPSubset.pl>) and ERA-Interim (see, <http://apps.ecmwf.int/datasets/data/interim-full-daily/levtype=sfc/>) to compare their results with those COSMIC RO data over the GBM basin.

3.3 Ocean-atmospheric indices

We used three ocean-atmospheric indices namely, (a) El Niño Southern Oscillation Index (ENSO), (b) Indian Ocean Dipole (IOD), and (c) quasi-biennial oscillation (QBO) that are commonly associated with significant fluctuations in UTLS temperatures. ENSO is commonly measured by sea surface temperature (SST) anomalies in the equatorial Pacific ocean, typically over (5°N–5°S, 120°–170°W), which is also known as Niño3.4 (see, Trenberth, 1990). ENSO events are said to occur if SST anomalies exceed 4°C for 6 months or more. Warm and cold ENSO phases are referred to as El Niño and La Niña events, respectively, which are represented by anomalous warming of the central and eastern tropical Pacific (warm phase), and vice versa. ENSO events are marked by significant variations in surface and upper-air conditions such as prolonged droughts and heavy rainfall events at the surface and anomalous warming or cooling of the UTLS region. Based on the Niño3.4 index obtained from the National Oceanic and Atmospheric Administration (NOAA, see, <http://www.esrl.noaa.gov/psd/data/climateindices/list/>), three El Niño events and four La Niña events have occurred between 2006 and 2013.

IOD is measured by difference of SST anomalies between the western (50°E to 70°E and 10°S to 10°N) and eastern (90°E to 110°E and 10°S to 0°S) equatorial Indian ocean, which is also referred to as Dipole Mode Index (DMI). Positive IOD events are identified by cooler than normal water in the tropical eastern Indian Ocean and warmer than normal water in the tropical western Indian Ocean and are associated with a shift of active convection from eastern Indian Ocean to the west leading to potentially higher than normal rainfall over parts of the Indian subcontinent. DMI indices obtained from <http://www.jamstec.go.jp/frsgc/research/d1/iod/> indicated four positive IOD events and two negative IOD events during the last 8 years. QBO is stratospheric phenomenon characterized by an east–west oscillation in stratospheric winds over a period of approximately 28 months (Baldwin et al., 2001). The QBO dominates variability of the equatorial stratosphere and is easily identified as downward propagating easterly (negative) and westerly (positive) wind regimes and commonly measured by an index computed based on zonal winds at 30 hPa or 50 hPa. A full QBO cycle consists of westerly and easterly phase. QBO indices at 30 hPa were download from NOAA and during the period 2006 to 2013, we found three complete QBO cycles.

3.4 Tropopause temperatures and heights

Due to the complex chemical composition and its response to the variability of troposphere and stratosphere, various methods have been used to define the tropopause such as *lapse-rate tropopause* (LRT), *cold point tropopause* (CPT), *dynamical tropopause* (IPV or isentropic potential vorticity), *ozone tropopause* (OT), and *100 hPa pressure level* (see, Holton et al., 1995; Pan et al., 2004). Of these, LRT has been identified as a key indicator of climate change as the height of LRT is sensitive to bulk changes in the thermal structure of the stratosphere and the troposphere (e.g., Santer et al.,

2003a; Sausen and Santer, 2003). Here, we used the LRT (simply referred as tropopause henceforth) based on definition outlined by the WMO (1957): “the lowest level at which the lapse rate decreases to 2°C/km or less, provided also the average lapse rate between this level and all higher levels within 2 km does not exceed 2°C/km.” The significance of tropopause as a climate indicator has been reported in a number of studies and many approaches have been taken to define the tropopause layer based on various atmospheric variables (e.g., temperature, potential vorticity, etc.). This study focusses on the interannual variability of thermal tropopause or the “lapse rate tropopause” (LRT) derived from COSMIC RO and MERRA data over the GBM basin. According to WMO (1957), LRT is the lowest level at which lapse rate decreases to less than 2 °C/km and the average lapse rate between the lowest level and anywhere above that level up to 2 km remains less than 2°C/km. COSMIC RO data obtained from CDAAC already contain the derived tropopause parameters (height and temperature). The tropopause heights and temperatures from COSMIC data have already been computed by CDAAC, while MERRA also provides tropopause temperature and pressure based on the WMO (1957) definition. We did not use ERA-Interim here because we believe that assimilation of GNSS RO data could likely cause bias in trend estimates and variabilities, which will be reported later. The tropopause height, h_{LRT} (in km) for MERRA was approximated from the tropopause pressure, p (in hPa) using the following relationship (PSAS, 2004):

$$h_{LRT} \equiv 44330.8 - 4946.54 \times p^{0.1902632}. \quad (1)$$

3.5 Principal Component Analysis (PCA)

COSMIC RO mission provides an excellent opportunity to assess the interannual variability of the UTLS (subtropical) region. With an average of ~ 576 useful RO profiles per month that are uniformly distributed across the GBM river basin since August 2006 (see, Figure 2), COSMIC RO provides an excellent opportunity to assess examine interannual variability of temperature in the UTLS region. The interannual variability of UTLS temperature was carried out based on the monthly COSMIC RO data and were compared with MERRA products from August 2006 to December 2006. Monthly accumulated COSMIC RO data were ~~must be~~ interpolated to a spatial resolution of $0.5^\circ \times 0.5^\circ$ over 14 standard pressure levels from 500-10 hPa (or 7.5-31 km) using the ordinary kriging method (see details in the supplementary material). gridded for each month over the region to provide a uniform spatial pattern and to provide a fair comparison to MERRA data. The monthly gridded temperature data of COSMIC were averaged for the two regions: (a) UT (400-150 hPa or ~ 7.5 -14.2 km) and (b) LS (70-30 hPa or ~ 18.7 -24.0 km). The mean temperature data for the two regions were then interpolated to a spatial resolution of $0.5^\circ \times 0.5^\circ$ using the “ordinary kriging” method (details in the Appendix). The geostatistical kriging methods have been shown to be more robust and spatially more reliable than other existing methods such as inverse-distance-weighting, Thiessen Polygons (see, e.g., Goovaerts, 2000; Zhang and Srinivasan, 2009). The UTLS temperature for the MERRA data were obtained by averaging the layers similar to COSMIC data for the same

time period. To study the interannual variations of temperature at various pressure levels, monthly temperature at each grid cell were deseasonalized by removing the time mean from each month. We also applied Principal Component Analysis/Empirical Orthogonal Functions (PCA/EOF, Lorenz, 1956; Preisendorfer, 1988) to the deseasonalized tropopause height and temperature to extract multiple variability modes associated with various atmospheric-oceanic mechanisms. PCA (hereinafter) is one of the widely used data exploratory tools used in atmospheric/oceanic science that allows for a space-time display of spatio-temporal data such as temperature in here, in a very few modes. PCA is multipurpose and have been used to study the impact of ENSO and QBO modes at various levels of the atmosphere including the tropopause (see, Randel et al., 2000; Gettelman et al., 2001). The central idea of PCA is to find a set of orthogonal spatial patterns (or EOFs) along with a set of associated uncorrelated time-series or principal components (PCs) that captures most of the observed variance (expressed in %) from the available spatio-temporal data (e.g., temperature). In summary, the EOF decomposition can be written as $\mathbf{X}_{(t,s)} = \mathbf{P}_{(t,n)} \mathbf{E}_{(s,n)}^T$ where $\mathbf{X}_{(t,s)}$ is the space (s)-time (t) data with its time-mean or annual cycle removed, $\mathbf{E}_{(s,n)}$ contains the EOFs with n number of retained modes, and $\mathbf{P}_{(t,n)}$ are the PCs obtained by projecting the original data ($\mathbf{X}_{(t,s)}$) on the orthogonal base-functions $\mathbf{E}_{(s,n)}$, i.e., $\mathbf{P}_{(t,n)} = \mathbf{X}_{(t,s)} \mathbf{E}_{(s,n)}$. This method can be applied at various stages of the data in order to find any meaningful links to various dynamics of the climate system using a subset of PCs.

The interannual variability of UTLS temperature was assessed by removing the annual and semi-annual cycles from the time-series of COSMIC and MERRA based on the multilinear regression model. For example, if $\mathbf{X}_{n \times m}$ is a time series of COSMIC or MERRA data with $n = 89$ months and $m = 1404$ grid cells over the GBM river basin, the residual time series ($\hat{\mathbf{X}}_{n \times m}$) can be obtained by:

Equation 4

where $x(l, j)$ represents an entry of \mathbf{X} from $l = 1, \dots, n$ and $j = 1, \dots, m$, and $\hat{\beta}_2$ to $\hat{\beta}_5$ are the regression coefficients representing the linear annual ($\hat{\beta}_2, \hat{\beta}_3$) and seasonal ($\hat{\beta}_4, \hat{\beta}_5$) cycles derived by fitting a multilinear regression model using the least squares adjustment technique.

4 Results and Discussion

4.1 Seasonal and interannual variability of UTLS temperature

First, we compared COSMIC profiles (both dry and wet profiles) with temperature and refractivity profiles from 24 radiosonde stations across the GBM basin from August 2006 to December 2013 with 18 of them located within the Indian territory. While the results (see, Appendix A) confirmed those of the previous studies (e.g., Sun et al., 2010; Kumar et al., 2011; Ansari et al., 2015) with anomalously warm bias (up to 4°C) for those old radiosondes (IMD-MK4) over India, results from recently upgraded three radiosondes (over India) also showed reduced but substantial warm bias (up

to 2.7°C) with very high standard deviations in the UTLS region (see supplementary material). This suggests that newly installed GPS-based sondes still did not achieve the standard that is shown by other radiosonde types despite their recent acceptance in the global weather assimilation systems (see, Kumar et al., 2011). This further highlights the importance of using RO data in both global
 420 assimilation systems and climate variability studies to improve our understanding of upper atmospheric conditions and weather forecasts over the region.

Figure 4 shows the regional mean temporal evolution of UTLS temperature with each time series plotted as anomalies (time mean removed). The temperature anomalies scale between $\pm 6^\circ\text{C}$ and shows largest anomalies above 50 hPa (in the lower stratosphere) and below 200 hPa (in the upper
 425 troposphere). A strong seasonal cycle is evident in the lower troposphere (below 200 hPa) and the stratosphere (above 70 hPa) whereas the seasonal cycle is found to diminish at the tropopause region (150-70 hPa) in some years (2008/2009, 2011/2012). The three datasets (COSMIC, MERRA, and ERA-Interim) agree very well above 200 hPa where water vapour is negligible. Below 200 hPa, however, COSMIC “dry” profiles (Figure 4a) show anomalously cold bias compared to the reanalysis
 430 products (Figure 4b-c), where priori information (background data) is required to retrieve humidity and temperature profiles. The relative difference between COSMIC RO and reanalysis products were found to be very similar with 1.23°C and 1.22°C for MERRA and ERA-Interim, respectively between 200 hPa and 70 hPa while the differences between MERRA and ERA-Interim was $\pm 0.5^\circ\text{C}$. The annual cycle of temperature was plotted for four pressure levels: (a) 200 hPa, (b) 100 hPa, (c) 70
 435 hPa, and (d) 50 hPa in Figure 5 to estimate absolute bias in reanalysis products. The seasonality of temperature was captured very well at all pressure levels with MERRA and ERA-Interim showing warm bias at all pressure levels. Both the reanalysis products showed warm bias during monsoon period (by $\sim 1^\circ\text{C}$) in the troposphere (200 hPa, Figure 5a), consistent warm bias at 100 hPa (often used as proxy for tropical tropopause, Figure 5b), and by up to 2°C at 70 hPa (Figure 5c). The two
 440 reanalysis products showed quantitatively similar patterns except at 100 hPa where ERA-Interim showed smaller bias with COSMIC RO during the monsoon period, probably due to assimilation of GNSS RO data.

[FIGURE 4 AROUND HERE.]

[FIGURE 5 AROUND HERE.]

445 Interannual variations were also captured during the last 8 years with relatively lower temperature in the troposphere in 2009/2010 winter and early 2013, and low stratospheric temperature during 2007/2008, 2008/2009, and 2012/2013 winters. These variations are clearly shown by removing their mean annual cycle as shown in Figure 6 where warm (2006/2007, 2009/2010, and 2010/2011) and cold (2007/2008, 2008/2009, 2011/2012, and 2012/2013) temperatures were recorded at various
 450 levels in the stratosphere. A very warm (up to 1.5°C) temperature was also recorded at the tropopause level in 2006/2007, 2009/2010, and 2012/2013. These warm/cold anomalies are mainly driven by

various atmospheric/oceanic phenomenon that affect the global climate including the troposphere and stratosphere e.g., ENSO, QBO, and possibly local SST anomalies. The warm anomalies at the tropopause level during 2006/2007, 2009/2010, and 2012/2013 coincides with warm (El Niño) ENSO phase, while anomalously warm temperatures during 2009/2010 and 2010/2011 coincides with the stratospheric sudden warming (SSW) events. SSW are stratospheric events where polar vortex of westerly winds in the winter polar region (Northern Hemisphere) slows down or even reverses direction over the course of a few days, which are accompanied by sudden rise in stratospheric temperature by several tens of °C (e.g., Hansen et al., 2014). These anomalously warm temperatures in the upper stratosphere (above 30 hPa) were associated with very cold temperature anomalies between the tropopause and 50 hPa with a decrease of about 5°C from its temporal mean during the 2008/2009 strong SSW event. The results are consistent with those from (Resmi et al., 2013), who used ERA-Interim and observations from six radiosonde stations across India. Their study also found that surface temperatures react strongly to these major SSW events. All the three datasets showed quantitatively similar interannual variations at all pressure levels from 500 hPa to 10 hPa indicating that both MERRA and ERA-Interim products were of considerably high quality despite their low vertical resolution. This consistency has also been already noted in ERA-Interim by Poli et al. (2008, 2010) on a global scale. Figure 9 shows the seasonal variability of temperature in the UTLS region over the GBM river basin from August 2006 to December 2013. The temperature in the UT region was marked by a strong seasonal pattern indicating a difference of up to 10°C between the lower and the upper peaks (Figure 9a and b). The strong seasonality gradually diminishes and became nearly constant in the tropopause layer between 150 hPa and 70 hPa (14–18.5 km) indicating a much wider tropopause belt in the region. This supports the view that tropopause is no more a thin layer (Fueglistaler et al., 2009). The temperature pattern in the stratosphere (above 18.5 km) was relatively stable without much seasonality but exhibited sudden fall in temperature during the early months of 2008, 2009, and 2013. These cooling events have been reported to be associated with Sudden Stratospheric Warming (SSW) events in the winter polar regions (Hansen et al., 2014). The stratosphere responds to major global climatic events such as Brewer-Dobson circulation, solar radiations, and natural and man-made aerosol forcings (e.g., Fueglistaler et al., 2009), and have been found to influence global weather conditions in the lower troposphere (e.g., Foelsche et al., 2008; Seidel et al., 2011) including persistent occurrence of thin cirrus clouds over the Indian subcontinent (see, Sridharan et al., 2011). The SSW events in the winter polar region have been found to be associated with significant cooling (of about 1°C) of the stratosphere over low latitude and equatorial regions (Fritz and Soules, 1972).

[FIGURE 6 AROUND HERE.]

We also plotted temperature anomalies at (a) 200 hPa, (b) 100 hPa, (c) 70 hPa, and (d) 50 hPa in Figure 7a-d together with ocean-atmospheric indices in Figure 7e. The 200 hPa temperature anomalies clearly shows the influence of 2009/2010 El Niño event (Figure 7a) with a decrease of ~1.5°C

in January 2010. The 2009/2010 El Niño event commenced in May 2009, reaching its peak in late
 490 December 2009 before slowing down in the first quarter of 2010. The tropospheric (200 hPa) tem-
 peratures are negatively correlated with 100 hPa, which is visible especially during the major ENSO
 events of 2009/2010 (Figure 7b). The 100 hPa level, which is often used as proxy for tropopause, also
 shows some pattern of QBO in 2008/2009 and 2010/2011. However, it indicated warm temperature
 in 2013 despite continuing periods of negative QBO. The temperature anomalies at 70 hPa and 50
 495 hPa (Figure 7c-d) primarily indicates the temporal structure of major SSW events that were observed
 in Figure 6. One major SSW event (in 2009/2010) and two major SSW events (2010/2011) have oc-
 curred during the last 8 years, which is clearly seen at 50 hPa (lower stratospheric layer considered
 to be very close to the onset of QBO). The stratospheric temperature anomalies at 70 hPa and 50
 hPa also shows a decrease of temperature by about 1°C in 2007, which did not correspond well with
 500 any of the indices. Correlation coefficients between temperatures at these four pressure levels and
 atmospheric/ocean indices given in Table 1 indicates that ENSO dominates its influence in the UTLS
 region showing maximum influence in the tropopause region with a correlation of 0.82 (for lag of
 1 month). Warmer (colder) SST leads to stronger (weaker) convection resulting in colder (warmer)
 tropopause temperatures and are negatively correlated with tropospheric temperatures. The correla-
 505 tion results were reported only for COSMIC RO as both MERRA and ERA-Interim were found to
 be highly skillful in depicting the interannual variability (see, Table 1).

[FIGURE 7 AROUND HERE.]

It is worth mentioning that IOD mode was found to be significantly correlated (at 95% confidence
 interval) to the ENSO mode during the period 2006 to 2013 with a correlation coefficient of 0.42.
 510 Nevertheless, the relationship between IOD and temperature is significant only in the troposphere
 where convection is maximum. For example, correlation between IOD and 200 hPa was -0.42 (see
 Table 1) whereas it increased to -0.53 at 400 hPa. Temperature at 100 hPa (or the proxy tropopause)
 level generally provides a good approximation of the QBO signal (e.g., Reid and Gage, 1985; Randel
 et al., 2000; Liang et al., 2011) such that its correlation was reported as high as 0.86 over the equato-
 515 rial region from 2004 to 2010 (see, Liang et al., 2011). However, the relationship between QBO and
 temperature at 100 hPa was found to be negative and substantially low, which could be due to
 prolonged westerly phases from June 2008-January 2010 followed by a step easterly phase peaking
 in June 2010. The correlation between QBO and 100 hPa temperature was 0.47 and reaches to 0.53
 at 50 hPa, both of which are still statistically significant at 95% confidence interval. The relationship
 520 between QBO and Niño3.4 diminished after mid-June 2009 implying that its influence over tropo-
 sphere upwelling in the Indian monsoon region (see e.g., Chattopadhyay and Bhatla, 2002; Resmi
 et al., 2013; Liang et al., 2011) may have also altered due to stronger easterly phases and prolonged
 westerly phases.

Trends in temperature were calculated from the deseasonalized temperature anomalies using the
 525 non-parametric Sen's slope estimator (Sen, 1968) and their significance were tested at 95% confi-

dence level using the Mann-Kendall's non-parametric test (Mann, 1945; Kendall, 1962). The linear trends estimated from four pressure levels shown in Figure 7 is given in Table 2. Based on Figures 7a-d, we found a slight increase in temperature ($0.02 \pm 0.02^\circ\text{C}$ based on COSMIC RO) in the upper troposphere (at 200 hPa level), although not significant, and decrease in temperature ($-0.04 \pm 0.05^\circ\text{C}$ based on COSMIC RO) at the tropopause level (indicated by the 100 hPa level). We found a pronounced cooling (-0.07 ± 0.05 based on COSMIC RO) at 70 hPa level compared to 50 hPa level ($-0.02 \pm 0.04^\circ\text{C}$, also based on COSMIC RO) during the past 8 years. This warming (cooling) of the troposphere (stratosphere) has been well simulated by the global climate models (GCMs) and is believed to be in response to the increasing concentrations of greenhouse gases (e.g., Santer et al., 2005; IPCC, 2007; Santer et al., 2008; IPCC, 2013; Lott et al., 2013). These trends were also found to be very consistent in the two reanalysis products (MERRA and ERA-Interim) except at 100 hPa level where MERRA data did not show any trend (see, Table 2). The uncertainties in trend estimates were relatively larger than the trend themselves due to the short time-span but nevertheless the trends are clearly visible at different levels (see Figure 7).

The MERRA data (Figure 9b) was found to agree very well above 12.5 km indicating a difference of only $\pm 1^\circ$ (Figure 9c) but indicated large differences in the tropospheric region with a difference of up to $\pm 3^\circ$. The amplitudes of COSMIC RO data were found to be lower in the lower troposphere with a slightly delayed temperature maximum in the region. The lower amplitudes in COSMIC RO (Figure 9a) could have resulted from the low resolution background information used to retrieve RO temperature in the troposphere (Kuo et al., 2004).

To further understand the dynamics of the UTLS region over the GBM basin, the interannual variability of temperature of the UTLS region was assessed. The temporal temperature patterns were derived by removing the annual and semi-annual cycles from the basin-averaged time series of COSMIC RO and MERRA data (see, Eq. 4). The de-seasonalised time series were compared with large-scale ocean-atmospheric phenomena such as ENSO and IOD, which were found to significantly influence the seasonal climate fluctuations in the GBM river basin (see, e.g., Chowdhury and Ward, 2004, Ashok and Saji, 2007). ENSO is commonly represented by sea surface temperature (SST) anomalies such as those within the Niño3.4 region (5°N – 5°S , 120° – 170°W) (Trenberth, 1990), while IOD is commonly measured by the difference between SST anomalies in the western (50°E – 70°E and 10°S – 10°N) and eastern (90°E – 110°E and 10°S – 0°S) equatorial Indian Ocean, which is referred to as Dipole Mode Index (Saji et al., 1999). Monthly ENSO index (Niño 3.4) from the Climate Prediction Center (CPC) and DMI (as IOD index) from the Low-latitude Climate Prediction Research were used.

In addition, comparisons were also made with Quasi-Biennial Oscillation (QBO) index at 30 hPa, which were extracted from the NOAA website. QBO or formally known as Singapore Winds is a quasiperiodic oscillation of the equatorial zonal wind between the easterlies and westerlies in the tropical stratosphere where the downward propagating winds are finally dissipated at the tropical

tropopause region, with a mean period of about 28 months (Baldwin et al., 2001). The variability of QBO in the lower stratospheric temperature can induce interannual variability in the tropopause temperature (Baldwin et al., 2001). QBO is measured by an index derived from the zonally averaged easterlies at 50–30 hPa above the equatorial region.

Figures 10a and 10b shows the interannual variability of temperature in the UT and LS, respectively, together with the corresponding temporal patterns of QBO, ENSO (Niño3.4), and IOD (DMI) over the period from August 2006 to December 2013. The temporal patterns of temperature in UT and LS region were found to exhibit the patterns of all three climate indices with varying degree of magnitudes. The ENSO activity heightened during the past 5 years with two major warm phases (i.e., El Niño or +ive Niño3.4) in 2006–2007 and 2009–2010 and four major cold phases (i.e., La Niña or -ive Niño3.4) during the periods 2007–2008, 2008–2009, 2010–2011, and 2011–2012 (see, Figure 10). These cold (warm) ENSO phases are associated with extreme drought conditions (flooding) in the GBM river basin with further contribution from IOD activities, which may also act independently during the neutral ENSO periods (see, e.g., Chowdhury and Ward, 2004, Ashok and Saji, 2007).

The stratospheric temperature showed a maximum amplitude of -3°C during the winter of 2008–2009 (Figure 10a) corresponding to the major SSW event (Resmi et al., 2013, Hansen et al., 2014) whereas the maximum amplitude (3°C) of tropospheric temperature was found to occur in the winter of 2011–2012 corresponding to a moderate La Niña period (Figure 10b). Similarly, the stratospheric cooling in the winter of 2012–2013 were associated with a major SSW event but has negligible impact on the tropospheric variability. The stratospheric temperature increases (decreases) during the positive El Niño (La Niña) periods (Figure 10a) while the tropospheric temperature showed the opposite, indicating an increase in temperature during the warm ENSO phase (Figure 10b). Thus, both stratospheric and tropospheric temperature shows very good correlation with ENSO pattern with a magnitude of 0.44 (for stratospheric temperatures) and -0.62 (for tropospheric temperatures) based on the COSMIC RO data even for a very short period of time (see, Table 4). The MERRA data showed a slightly better correlation with ENSO but indicated a lag of approximately one month with respect to the tropospheric temperature. This lag can be found especially during the periods of 2008–2009, 2010–2011, and 2013 but generally agrees very well with COSMIC RO data.

[FIGURE 10 AROUND HERE.]

The relationship between IOD and UTLS was found to follow the ENSO pattern indicating positive correlation during the warm ENSO phases and negative correlation during the cold phases of ENSO (see, Figure 10). IOD is also a major ocean-atmospheric event in the tropical Indian ocean (see, e.g., Chowdhury and Ward, 2004, Ashok and Saji, 2007) and was found to have large impact on the tropospheric temperature variability. The correlation between IOD and tropospheric temperature based on the 89 months of COSMIC RO data was -0.59 with a lag of 7 months (see, Table 4). Similar results were shown by MERRA data for the same lag period. Since QBO is a stratospheric phenomenon, it has greater influence on the stratospheric temperature than on the tropospheric tem-

600 perature. As a result, QBO has been found to be highly correlated with the stratospheric temperature (0.5 to -0.5).

[TABLE 4 AROUND HERE.]

4.2 Trends and variability of tropopause heights and temperatures

While it is possible to derive interannual variability of the tropopause based on the 100 hPa level, 605 Seidel et al. (2001) reported that it is a poor surrogate of tropical tropopause due to significantly lesser spatial and temporal variability than the heights of the LRT and CPT. In particular, their study also showed that 100 hPa level resides in the stratosphere during the northern hemisphere (NH) summer and in the troposphere during the NH winter, thus, indicating warmer temperatures than LRT and CPT. In this section, we use PCA to examine the variability of tropopause (i.e., LRT 610 tropopause) parameters (temperatures and heights) from COSMIC RO and MERRA over the GBM basin. The spatial domain shown in Figure 1 falls within the tropics and the subtropics where the tropopause height (temperature) is considered to be around 16 km ($\sim -82^{\circ}\text{C}$ close to the equator) (e.g., Reid and Gage, 1985; Randel et al., 2000; Seidel et al., 2001). The annual mean and standard deviation of tropopause temperatures and heights over the region are plotted in Figures 8 and 9 615 to show the spatial variability of the tropopause. The tropopause is generally colder (higher) in south (closer to the equator) reaching a minimum (maximum) of -81.5°C (16.9 km) over southern Myanmar (Figures 8a and 9a). While the temperature gradually increases from south to north (from -81.5°C to -69.5°C , based on COSMIC RO in Figure 8a), its heights are more or less homogenous at around 16.8 km below 29°N with its boundary roughly falling on the northern boundaries of Bhutan. 620 However, its height changes steeply by around 2 km from 29°N to 35°N , which also indicated the highest standard deviation (~ 1.8 km, Figure 9b). In this region, the standard deviations of up to 6°C were recorded in COSMIC RO data (Figure 8b).

[FIGURE 8 AROUND HERE.]

[FIGURE 9 AROUND HERE.]

625 The tropopause over the GBM basin often reaches as high as 18 km in response to the Indian summer monsoon when intense convective activities occur and as low as 10 km in winter due to weak convection. The spatial patterns of tropopause shown by MERRA were consistent with COSMIC RO but were found to be more zonally homogenous, warmer (by up to 4°C in the north) and lower (by ~ 1 km) over the region. This warm bias was also observed in ERA-Interim at 100 hPa (see Figure 630 5b) but was lower than MERRA especially during the monsoon. The impact of warm (and lower) tropopause in the reanalysis over the region could perhaps lead to underestimation of monsoon rainfall as higher tropopause indicate deeper convection and thus, more rainfall. The annual cycle of tropopause temperatures and heights of COSMIC RO and MERRA are shown in Figure 10. The

area-averaged temperatures (heights) of COSMIC RO reaches minimum (maximum) in June while
 635 MERRA shows large (but consistent) warm bias (1.0-2.5°C) and significantly lower height (by up
 to 1.2 km from May to December). MERRA also shows tropopause temperature minimum in July
 instead of June (Figure 10a). The bias in tropopause height may partly related to our approximation
 based on Eq. 1 but it should be noted that errors in tropopause heights cause large errors in its
 temperature due to the lapse-rate criterion. The warm bias in observed in reanalysis products were
 640 thought to mainly stem assimilation of large observations from aircrafts and satellites (see e.g., Dee
 et al., 2011, and references therein). The uncertainties in temperature and height indicated by error
 bars in Figure 10 shows that there are large variations in tropopause (temperatures and heights)
 especially during winter and spring and could be related to diurnal variations (Mehta et al., 2010).

[FIGURE 10 AROUND HERE.]

645 The seasonal and interannual variations of tropopause temperatures and heights over the GBM
 river basin were investigated. Figure 11 shows the frequency distribution of tropopause temperatures
 and heights based on the COSMIC RO data only. The tropopause exhibited a clear seasonal variation
 over the GBM basin with lower and warmer tropopause during winter (DJF, i.e., Figures 11a and
 9e), and higher and colder tropopause during the summer (JJA, i.e., Figure 9c) and autumn (SON,
 650 i.e., Figure 9d). The tropopause height varied between 10 km and a little over 18.5 km corresponding
 to a temperature of -40°C and around 85°C. Large variations were seen especially during the spring
 (MAM) with a standard deviation of 9.6°C and 2.2 km, respectively (Figures 9b and 9f). This high
 variation of tropopause in spring could be due to high diurnal (day and night) variations, which tend
 to be in the order of ~1 km and ~3°C over the region (Mehta et al., 2010).

[FIGURE 9 AROUND HERE.]

655 To further illustrate the seasonal variations of the tropopause, Figures 12 and 13 shows the spa-
 tial distribution of annual and semi-annual amplitudes of tropopause temperatures and heights (i.e.,
 mean annual variation) derived from MERRA and COSMIC RO data. These annual and semi-an-
 nual amplitudes were derived from the multilinear regression model described in Eq. 4. The highest
 660 amplitudes were found over the subtropics (north of 26°) where the tropopause temperatures were
 found to vary by almost 8°C (Figure 12a and 12c) and tropopause heights varied by up to 2 km in the
 same region (Figures 13a and 13c). The semi-annual variations of tropopause temperatures (Figures
 12b and 12d) and heights (Figures 13b and 13d) were relatively small (with a maximum of 0.4°C
 and 0.15 km, respectively). It is interesting to note that the magnitude of variations in tropopause
 665 temperatures increased sharply along 26°N (Figures 12a and 12c) while the tropopause heights' vari-
 ations were found to be more steeper along northern boundary of the GBM river basin. The spatial
 patterns of amplitudes derived from MERRA data as shown in Figures 12c and 13c were found to
 be consistent with COSMIC RO data, but MERRA indicated larger temperature variations while its
 height variations were less than 1.5 km.

[FIGURE 12 AROUND HERE.]

[FIGURE 13 AROUND HERE.]

To be more precise on the seasonal variation of tropopause over the region, the mean annual cycle of tropopause temperatures and heights with their standard deviations are plotted in Figure 14. The seasonal variation of tropopause indicated a strong annual cycle following the Indian monsoon pattern over the GBM river basin. The minimum tropopause temperature of COSMIC RO data was found to occur during the peak monsoon period (July) while the maximum temperature was found to occur in January (Figure 14a). On the other hand, the tropopause height peaks in June and reaches its minimum in January (Figure 14b). The tropopause variations (represented by error bars) were found to be very small during the monsoon period (June–September) and substantially high from November to May. Such variations could be related to synoptic scale (day-to-day) variability of the regional atmospheric convection over the region (Mehta et al., 2010). The day-to-day variations can be particularly large when the small-scale convective activities dominate the regional atmosphere between November and May. Both the dataset indicated strong annual cycle but tropopause was found to be warmer (by $2\text{--}5^{\circ}\text{C}$) and lower (by 1 km) over the GBM basin. Earlier studies have also reported warm biases in reanalysis products compared to GNSS RO data and radiosonde observations (Randel et al., 2000).

[FIGURE 14 AROUND HERE.]

The annual cycle was removed from each grid cells to examine the interannual variability of tropopause parameters and linear trends were also calculated based on area-averaged time series anomalies over the period August 2006 to December 2013. The linear trend estimates and their uncertainties are given in Table 3. In general, tropopause appears to be cooling (increasing) at rate of $-0.039 \pm 0.05^{\circ}\text{C}$ (6.01 ± 5.02 meters) during the period (see Table 3), which is to some degree reflected in the MERRA product. However, MERRA shows negligible cooling compared to COSMIC RO whereas its height increase is exaggerated and are not consistent with the temperature decrease. The increasing (decreasing) tropopause heights (temperatures) has been consistently observed in GNSS RO retrieved parameters over the years at both global and regional scale (e.g., Schmidt et al., 2008, 2010; Khandu et al., 2011), which is evidently in response to enhanced warming in the upper troposphere and substantial cooling in the lower stratosphere.

While it is impossible to derive long-term trends and variability of the tropopause using COSMIC RO data, a short-term (89 months) interannual variability of the tropopause temperatures and heights has been carried out here. Since tropopause is a transitional layer between the troposphere and the stratosphere, both tropospheric activities such as ENSO and IOD and stratospheric activities such as QBO and SSW events can have significant influence on the temporal variations of tropopause heights and temperatures (Randel et al., 2000). The de-seasonalised temporal anomalies (using Eq.

4) (i.e., deviation from mean) of tropopause temperatures and heights of COSMIC RO data have been compared with those from MERRA data to assess the temporal variability of tropopause over the region.

To study the influence of global ocean-atmospheric phenomenon such as ENSO, QBO, and IOD on the interannual variation of tropopause heights and temperatures, we applied PCA the detrended temperature (and height) time-series anomalies to extract multiple leading modes of variability. PCA is particularly relevant here because tropopause is a transitional layer that responds to perturbations from both the troposphere and stratosphere, which makes it difficult to understand their variability modes. Figure 11 shows the EOFs (or spatial maps) for the first three leading modes of variability. The first EOF accounts for variability of $\sim 73\%$ (COSMIC RO) and $63\sim\%$ (MERRA) indicating positive anomalies (up to 1.1°C) across the GBM basin. The spatial patterns of EOF 1 appears rather symmetric about 29°N in COSMIC RO but seems to be shifted slightly southwards in MERRA (Figures 11a and 11d). Its corresponding PC shown in Figure 12a is found to be highly correlated with Niño3.4 index at 0.77 (COSMIC RO) and 0.78 (MERRA) with a lag of one month. Thus, the impact of ENSO is found to be maximum over the Himalayan region. We also found statistically significant correlation between PC 1 and IOD with a correlation of 0.35 for both COSMIC RO and MERRA (with a lag of 2 months) indicating that positive IOD events induces cooler tropopause. The correlation coefficients are provided in Table 4.

[FIGURE 11 AROUND HERE.]

[FIGURE 12 AROUND HERE.]

The second EOF (Figures 11b and 11e) shows a diagonal (dipole) pattern with positive (negative) anomalies in the northwest (southeast) and accounts for $\sim 10\%$ (COSMIC) and $\sim 18\%$ (MERRA) of variability. Its corresponding PC was found to be correlated with the QBO index at 0.40 (COSMIC RO) and 0.53 (MERRA) (at zero lag). It is not surprising that the relationship between PC 2 and QBO is rather low compared to the equatorial (or tropical) tropopause since the impact of QBO is maximum around the equator (between $\pm 15^{\circ}$). However, it is interesting to find that its impacts are diagonal over the region (from 2006-2013), which usually is symmetric around the equator (e.g., Reid and Gage, 1985; Randel et al., 2000; Gettelman et al., 2001). QBO is a well-known interannual signal observed in the tropical tropopause parameters such as tropopause responds to stratospheric variations to maintain the thermal wind balance. Liang et al. (2011) found a correlation of 0.86 between QBO and temperature anomalies (at 100 hPa level) in the equatorial region. The third EOF (Figure 11c and 11f) explains about 5% (COSMIC RO) and 10% (MERRA) of the variability and shows positive (negative) anomalies below (above) 30°N , although MERRA shows a diagonal dipole pattern similar to EOF 2. Their corresponding PCs were found to be moderately correlated with ENSO and IOD but not QBO.

The tropopause heights are negatively correlated with their temperature and therefore, should vary inversely with its temperature, i.e., increase in tropopause heights with drop in temperatures. The first three leading EOFs are shown in Figure 13 and their corresponding PCs are plotted in Figure 14. While tropopause temperatures shows maximum variation along 29°N, tropopause heights shows largest anomalies above 25°N (Figures 13a and 13d) in response to ENSO events indicating that its impacts are felt mostly in the subtropics. The correlation (see, Table 4) between PC 1 and Niño3.4 index was -0.74 (COSMIC RO) and -0.75 (MERRA). IOD also shows a modest relationship with a correlation of around 0.37 for both the datasets. The QBO structures over the region is rather complicated and difficult to explain but nevertheless follows its temperature pattern as shown in Figures 11b and 11e. The correlation between PC 2 and QBO index was higher for MERRA (0.53 at zero lag) compared to COSMIC RO, which did not capture the QBO signals very well. Nevertheless, it shows a modest correlation (0.36 at zero lag). We also computed trends based on the extracted ENSO and QBO modes but no significant trends were detected in tropopause temperatures and heights. Thus, decreasing (increasing) tropopause temperatures (heights) may be related to tropospheric warming (as evidenced by enhanced cooling at 200 hPa level) that could be induced by increasing concentrations of greenhouse gases. Since ENSO and IOD are somewhat related (see, also Ashok and Saji, 2007), it is difficult to separate the two modes in tropopause parameters but it should be noted that ENSO events dominate the tropopause variability in the region with maximum impacts in the subtropical region.

[FIGURE 13 AROUND HERE.]

[FIGURE 14 AROUND HERE.]

To show the influence of ENSO mode on the tropopause, we have plotted the seasonal mean time-series anomalies of tropopause temperatures and heights in Figure 15. Seasonal mean anomalies were obtained by multiplying EOF 1 and PC 1. Figure 15 shows that ENSO influences tropopause mainly during the winter (e.g., 2009-2010, 2012-2013) (when ENSO was at its peak). Nevertheless, it should be mentioned that maximum impact was also felt during autumn (in 2007 and 2011) and spring (in 2008) during both El Niño and La Niña periods. The largest anomaly was found in 2009/2010 winter where tropopause temperature (height) increased (decreased) by about 2°C (300 meters) due to a major El Niño event. La Niña periods (e.g., 2007/2008, 2010/2011) are mainly associated with above normal rainfall in the GBM basin, which is also associated with deep convections in the troposphere (see Figure 15). This deep convections are associated with colder and higher tropopause. QBO and SSW events are also closely related such that it also induces large tropopause perturbations, which is especially evident in PC 2 (Figures 12b and 14b) where tropopause showed maximum amplitude in 2008/2009 early spring.

[FIGURE 15 AROUND HERE.]

Figure 15 shows the interannual variability of tropopause temperatures and heights derived from COSMIC RO and MERRA data for the period between August 2006 and December 2006, as well as the indices of QBO, ENSO (Niño3.4), and IOD (DMI). The tropopause temperature of COSMIC RO data exhibited the patterns of ENSO (Niño3.4) and IOD (DMI) very well (Figure 15a) with a correlation of 0.65 and -0.38, respectively, which were equally represented by the MERRA data (Table 5). While ENSO lags tropopause temperature by one month, IOD was found to appear earlier by 6 months as indicated by both the dataset. For instance, the tropopause warmed by about 2°C during the major El Niño events of 2009–2010 and a cooling of similar magnitude has occurred during the major La Niña periods of 2010–2011 (see, Figure 15a).

[FIGURE 15 AROUND HERE.]

While the tropopause cools as a result of major SSW events in the northern polar region, even though with a lesser magnitude in this study, the major SSW event of 2009 was found to have a large impact on the tropopause heights (Figure 15b). The tropopause height increased by more than 2 km over the region as indicated by the MERRA data. However, COSMIC RO data showed an increase of only about 1 km. ENSO and IOD events were still found to dominate the temporal variation of tropopause heights in the region, which showed a correlation of -0.52 and 0.33 (based on COSMIC RO data) and lag (lead) of one (six) months, respectively. MERRA data indicated a slightly higher correlation with ENSO and IOD. The increase in tropopause temperature during the El Niño conditions were associated with an equivalent decrease in tropopause heights (e.g., 2009–2010). Furthermore, the tropopause heights showed a similar decrease during the early months of 2013 after a moderate El Niño event (with contributions from IOD).

[TABLE 5 AROUND HERE.]

The QBO is a well-known stratospheric phenomenon, which has been reported to have greater influence on the tropical tropopause characteristics (Reid and Gage 1985, Randel et al., 2000). The relationship between tropopause and QBO signal over the GBM river basin (in the sub-tropical region) was found to be quite complex mainly because of the ~28 month cycle of the QBO signal (Baldwin et al., 2001), which cannot be properly captured in the temporal period defined in this study. The peak-to-peak time differences of maximum correlation (0.4 to -0.5) between tropopause (temperatures and heights) and QBO signals was around 30 months, consistent with the cycle of QBO signal (figures not shown).

5 Conclusions

Several GNSS RO missions were launched in the past decade delivering thousands of to provide high-quality, global observations of the Earth's atmosphere (ionosphere, stratosphere, and troposphere)

for various weather and climate applications. This study examined the interannual variability of temperature in the UTLS region **including tropopause temperatures and heights** as well as the tropopause over the GBM river basin in South Asia **based on using** 89 months (August 2006 to December 2013) of COSMIC RO data **and two global reanalysis products (MERRA and ERA-Interim)**. The GBM basin received a total of 59,419 RO profiles from six COSMIC satellites between April 2006 and December 2013, with an average of ~ 576 well-distributed profiles/month from August 2006 to December 2013. More than 56% of the profiles reached at least 1.5 km above the mean sea level height. ~~Radiosonde observations from 24 stations in and around the GBM basin were compared with COSMIC RO data to assess the quality of on-going monitoring work in the region. ShangE/China radiosondes showed the best agreement with a mean temperature difference of -0.06°C and standard deviation of 1.44°C followed by ShangM/China and those over Bangladesh. The IMD radiosondes still exhibited large warm biases and anomalously high variations in the UTLS region even after upgrading their radiosondes at three stations. However, from the data period used in this study, the mean temperature differences were observed to have reduced by more than half (2.72°C to 1.20°C) after upgrading them. While there are substantial absolute warm bias (by up to 2°C at 200-50 hPa level) in MERRA and ERA-Interim in the UTLS region, they were found to be consistent over time resulting in a relative bias of $\pm 0.5^{\circ}\text{C}$. This enabled accurate representation of interannual variability of the UTLS temperature despite low vertical resolution. In the upper troposphere (at 200 hPa level), COSMIC RO data (dry profiles) showed a cold bias of around 1°C in the peak monsoon period. The UTLS temperature showed considerable interannual variability in the past 8 years (2006-2013) as well as modest changes in tropospheric and stratospheric temperatures. The cold (warm) anomalies in the upper troposphere indicated by 200 hPa level (tropopause region indicated by 100 hPa level) coincides with the warm ENSO phase (El Niño events) while SSW signals were seen in the stratospheric temperature anomalies. In particular, temperature at 200 hPa reduced by $\sim 1.5^{\circ}\text{C}$ during the last major El Niño event of 2009/2010. The SSW signatures were captured best at 50 hPa level, which was marked by one major SSW event (2008/2009 winter) and two minor SSW events in 2010/2011 leading to decrease in temperature at the tropopause region. ENSO has the maximum influence around the tropopause region (indicated by 100 hPa level) with a correlation of 0.82 (at 1 month lag) while QBO showed maximum influence at the 50 hPa level (with a correlation of 0.53).~~

The relationship between ENSO and QBO was reported to be considerably high between 2004 and 2008 (see, Liang et al., 2011) but has since diminished by mid-2008 due to a persistent westerly phase that lasted for 21 months from June 2008 to January 2010. Thus, the combined impacts of ENSO and QBO are not well understood. IOD, although considered to be relatively mild compared to ENSO, there exists significant correlation between Dipole Ocean Index (DMI) and temperature at 200 hPa level (with a correlation of -0.42) indicating that IOD impacts are felt mostly in the troposphere. In general, we found an upper tropospheric warming and lower stratospheric cooling with highest warming (cooling) at 200 hPa level (70 hPa level). These trends are consistent with

existing global warming trends and has been documented previously by many studies (see, e.g., IPCC, 2007, 2013, and references therein). The trends and temporal variations were well captured by both MERRA and ERA-Interim. It should be noted however that, trends are more pronounced in the UTLS region than in the lower tropospheric or the surface (Randel et al., 2000; Gettelman et al., 2001; Seidel et al., 2011).

The tropopause temperatures and heights derived from COSMIC RO and MERRA were investigated in detail due to their perceived importance in climate detection and attribution studies (see, e.g., Santer et al., 2003a, 2008; IPCC, 2007). The tropopause temperatures gradually increased from south to north (from -81.5°C to -69.5°C), while the tropopause heights were found to more or less homogenous over the region (at 16.8 km), although a step decline in heights was observed above 29°N . It should be noted however, that both tropopause temperatures and heights indicated significant seasonal variability with its height reaching as high as 18.5 km during the peak monsoon period. The temperature, as mentioned was found to be warmer (by up to 4°C) and lower (by 1 km) in MERRA and ERA-Interim products. Trends in tropopause temperatures and heights were consistent with the overall UTLS temperature (especially the 100 hPa level) trends indicating a decrease (increase) in temperatures (heights). These trends indicate that tropopause is sensitive to global change and is detectable even on a shorter time period. One potential impact due to increasing tropopause height is increase in water vapour in the lower stratosphere as it allows larger saturation mixing ratios to enter the stratosphere.

Using PCA, we extracted the interannual variability modes of the regional tropopause temperatures and heights. The results showed continued dominance of ENSO (see e.g., Reid and Gage, 1985; Randel et al., 2000; Gettelman et al., 2001; Seidel and Randel, 2006; Liang et al., 2011) with anomalies of up to 1.1°C in the subtropics. ENSO explains about 73% (COSMIC RO) and 63% (MERRA) of the interannual variability, which is preceded by the QBO mode accounting for $\sim 10\%$ (COSMIC RO) and $\sim 18\%$ (MERRA) of the interannual variability. Their corresponding PCs, particularly PC 1 shows an accurate representation of the ENSO mode (represented by the Niño3.4 index) with a correlation of 0.77 (COSMIC RO) and 0.78 (MERRA) while PC 2 was correlated with QBO at 0.36 (COSMIC RO) and 0.53 (MERRA) against tropopause temperatures. Similar correlation values were found between tropopause height and ENSO/QBO modes but it should be noted that tropopause heights are inversely correlated with ENSO due to its inverse relation with temperature. ENSO impacts tropopause temperatures and heights mainly during the winter (e.g., 2009-2010, 2012-2013) (when ENSO is at its peak). The largest anomaly was found in 2009/2010 winter where tropopause temperatures (heights) increased (decreased) by about 2°C (300 meters) due to a major El Niño event. The IOD mode, on the other hand was moderately related to ENSO and hence were more related to PC 1. A positive IOD event is usually associated with the shift in active convection from eastern Indian ocean to western Indian ocean, leading to higher than normal rainfall over parts of the Indian subcontinent and East Africa while severe droughts affect the Indonesian region. Thus,

positive IOD events should be normally associated with cooler (higher) tropopause temperatures (heights).

The temporal anomalies of UTLS (400–30 hPa; 7.5–24.0 km) temperatures exhibited clear temporal patterns of ENOS/IOD modes while also representing the major sudden stratospheric warming (SSW) events of 2009 and 2013 very well through the stratospheric temperature anomalies. Overall, the tropospheric temperature anomalies indicated very good correspondence with ENSO (Niño3.4 index) and IOD (DMI index) with negative correlations of 0.62 and 0.59, respectively. The MERRA data performed equally well with even higher correlation in this study. Based on COSMIC RO data, the mean tropopause temperature was found to vary between -70°C to -80°C with an average height of about 15.5 km to 16.3 km from winter to summer over the GBM river basin, thus, exhibiting a strong annual cycle in the region. The annual amplitudes of tropopause temperatures varied considerably from the tropics to the sub-tropics (0°C to 5°C) while the corresponding tropopause heights varied from 0 km to 1.5 km.

Both tropopause temperature and height anomalies over the GBM river basin exhibited strong temporal patterns of ENSO indicating a correlation of 0.65 and 0.52, respectively, with a lag of one month, and were equally represented by the MERRA data. The IOD also indicated reasonably good correspondence with tropopause temperature and height with a correlation of 0.38 and 0.33, and with a lag of six and five months, respectively. While QBO has a well known interannual signal, which significantly impacts the variability of tropopause in the tropics, its correlation with tropopause over the GBM river basin varied between 0.4 to 0.5 with a peak to peak time difference of ~ 30 months. The tropopause heights were found to be sensitive to the recent SSW events of 2008–2009, but were not properly captured during the last two SSW events of 2009–2010 and 2012–2013 due probably to strong combined influences of ENSO and IOD events.

Acknowledgement

The first author is deeply grateful to Curtin Strategic International Research Scholarship, Curtin University (Australia) for funding his PhD studies. He is further grateful to Intergovernmental Panel of Climate Change (IPCC) for the scholarship. J. Awange appreciates the financial support from both Alexander von Humboldt and Japan Society of Promotion of Science for his stay at Karlsruhe Institute of Technology (Germany) and Kyoto University (Japan), respectively. E. Forootan is grateful for the research grant from the German Aerospace Center (DLR). The authors are highly grateful to the COSMIC Data Analysis and Archival Center (CDAAC, <http://cdaac-www.cosmic.ucar.edu/cdaac/>) for providing both COSMIC radio occultation profiles, regional radiosonde datasets, and re-analysis profiles used in this study. The authors are also thankful to the MERRA for providing high-resolution global atmospheric products for regional studies. This is a TiGeR publication number (XXX).

~~[Appendix moved to supplementary material.]~~

~~[FIGURE 16 AROUND HERE.]~~

References

- Ansari, M. I., Madan, R., and Bhaita, S.: Verification of quality of GPS based radiosonde data, *Mausam*, 66, 367–374, available at: metnet.imd.gov.in/mausamdocs/16632_F.pdf, 2015.
- Anthes, R. A.: Exploring Earth's atmosphere with radio occultation: contributions to weather, climate and space weather, *Atmos. Meas. Tech.*, 4, 1077–1103, doi:10.5194/amt-4-1077-2011, 2011.
- Anthes, R. A., Ector, D., Hunt, D. C., Kuo, Y. H., Rocken, C., Schreiner, W. S., Sokolovskiy, S. V., Syndergaard, S., Wee, T. K., Zeng, Z., Bernhardt, P. A., Dymond, K. F., Chen, Y., Liu, H., Manning, K., Randel, W. J., Trenberth, K. E., Cucurull, L., Healy, S. B., Ho, S. P., McCormick, C., Meehan, T. K., Thompson, D. C., and Yen, N. L.: The COSMIC/FORMOSAT-3 Mission: Early Results, *Bull. Amer. Meteor. Soc.*, 89, 313–333, doi:10.1175/BAMS-89-3-313, 2008.
- Ashok, K. and Saji, N. H.: On the impacts of ENSO and Indian Ocean dipole events on sub-regional Indian summer monsoon rainfall, *Natural Hazards*, 42, 273–285, doi:10.1007/s11069-006-9091-0, 2007.
- Awange, J. L.: GNSS Remote Sensing of the Environment, in: *Environmental Monitoring using GNSS: Global Navigation Satellite Systems*, p. 382, Springer Berlin Heidelberg, 2012.
- Baldwin, M. P., Gray, L. J., Dunkerton, T. J., Hamilton, K., Haynes, P. H., Randel, W. J., Holton, J. R., Alexander, M. J., Hirota, I., Horinouchi, T., Jones, D. B. A., Kinnersley, J. S., Marquardt, C., Sato, K., and Takahashi, M.: The quasi-biennial oscillation, *Reviews of Geophysics*, 39, 179–229, doi:10.1029/1999RG000073, 2001.
- Barros, A. P., Kim, G., Williams, E., and Nesbitt, S. W.: Probing orographic controls in the Himalayas during the monsoon using satellite imagery, *Nat. Hazards Earth Syst. Sci.*, 4, 29–51, doi:10.5194/nhess-4-29-2004, 2004.
- Bindoff, N. L., Stott, P. A., AchutaRao, K. M., Allen, M. R., Gillett, N., Gutzler, D., Hansingo, K., Hegerl, G., Hu, Y., Jain, S., Mokhov, I. I., Overland, J., Perlwitz, J., Sebbari, R., and Zhang, X.: Detection and Attribution of Climate Change, in: *Climate Change 2013: The Physical Science Basis. Contribution of Working Group I to the Fifth Assessment Report of the Intergovernmental Panel on Climate Change*, edited by Stocker, T. F., Qin, D., Plattner, G.-K., Tignor, M., Allen, S., Boschung, J., Nauels, A., Xia, Y., Bex, V., and Midgley, P., Cambridge University Press, Cambridge, United Kingdom and New York, NY, USA, 2013.
- Chattopadhyay, J. and Bhatla, R.: Possible influence of QBO on teleconnections relating Indian summer monsoon rainfall and sea-surface temperature anomalies across the equatorial pacific, *International Journal of Climatology*, 22, 121–127, doi:10.1029/2010JD014841, 2002.
- Chowdary, J. S., John, N., and Gnanaseelan, C.: Interannual variability of surface air-temperature over India: impact of ENSO and Indian Ocean Sea surface temperature, *International Journal of Climatology*, 34, 416–429, doi:10.1002/joc.3695, 2014.
- Chowdhury, M. D. R. and Ward, N.: Hydro-meteorological variability in the greater Ganges–Brahmaputra–Meghna basins, *International Journal of Climatology*, 24, 1495–1508, doi:10.1002/joc.1076, 2004.
- Chowdhury, M. R.: The El Niño–Southern Oscillation (ENSO) and seasonal flooding – Bangladesh, *Theoretical and Applied Climatology*, 76, 105–124, doi:10.1007/s00704-003-0001-z, 2003.

Cucurull, L., Derber, J. C., Treadon, R., and Purser, R.: Assimilation of Global Positioning System radio occultation observations into NCEP's Global Data Assimilation System, *Mon. Weather Rev.*, 35, 3174–3193, doi:10.1175/MWR3461.1, 2007.

Das Gupta, M., Das, S., Prasanthi, K., and Pradhan, P. K.: Validation of upper-air observations taken during the ARMEX-I and its impact on the global analysis-forecast system, *MAUSAM*, 56, 139–146, 2005.

Dee, D. P., Uppala, S. M., Simmons, A. J., Berrisford, P., Poli, P., Kobayashi, S., Andrae, U., Balmaseda, M. A., Balsamo, G., Bauer, P., Bechtold, P., Beljaars, A. C. M., van de Berg, L., Bidlot, J., Bormann, N., Delsol, C., Dragani, R., Fuentes, M., Geer, A. J., Haimbergere, L., Healy, S. B., Hersbach, H., Holm, E. V., Isaksen, I., Kållberg, P., Köhler, M., Matricardi, M., McNally, A. P., Monge-Sanz, B. M., Morcrette, J.-J., Park, B.-K., Peubey, C., de Rosnay, P., Tavolato, C., Thépaut, J.-N., and Vitarta, F.: The ERA-Interim reanalysis: Configuration and performance of the data assimilation system, *Quarterly Journal of the Royal Meteorological Society*, 137, 553–597, doi:10.1002/qj.828, 2011.

Foelsche, U., Borsche, M., Steiner, A. K., Gobiet, A., Pirscher, B., Kirchengast, G., Wickert, J., and Schmidt, T.: Observing upper troposphere–lower stratosphere climate with radio occultation data from the CHAMP satellite, *Climate Dynamics*, 31, 49–65, doi:10.1007/s00382-007-0337-7, 2008.

Fueglistaler, S., Dessler, A. E., Dunkerton, T. J., Folkins, I., Fu, Q., and Mote, P. W.: Tropical tropopause layer, *Rev. Geophys.*, 47, doi:10.1029/2008RG000267, 2009.

Gautam, R., Hsu, N. C., Lau, K. M., Tsay, S. C., and Kafatos, M.: Enhanced Pre-Monsoon Warming over the Himalayan-Gangetic Region from 1979 to 2007, *Geophysical Research Letters*, 36, doi:10.1029/2009GL037641, 2009.

Guttelman, A. and de F. Foster, P.: A Climatology of the Tropical Tropopause Layer, *Journal of the Meteorological Society of Japan*, 80, 911–924, doi:10.1029/2006JD007363, 2002.

Guttelman, A., Randel, W. J., Massie, S., Wu, F., Read, W. G., and Russell, J. M.: El Niño as a Natural Experiment for Studying the Tropical Tropopause Region, *J. Climate*, 14, 3375–339, doi:10.1175/1520-0442(2001)014<3375:ENOAAN>2.0.CO;2, 2001.

Goovaerts, P.: Geostatistical approaches for incorporating elevation into the spatial interpolation of rainfall, *Journal of Hydrology*, 228, 113–129, doi:10.1016/S0022-1694(00)00144-X, 2000.

Hansen, F., Matthes, K., Petrick, C., and Wang, W.: The influence of natural and anthropogenic factors on major stratospheric sudden warmings, *Journal of Geophysical Research*, 119, 8117–8136, doi:10.1002/2013JD021397, 2014.

Healy, S. B. and Thépaut, J.-N.: Assimilation experiments with CHAMP GPS radio occultation measurements, *Q. J. R. Meteorol. Soc.*, 132, 605–623, doi:10.1256/qj.04.182, 2006.

Ho, S. P., Zhou, X., Kuo, Y. K., Hunt, D., and Wang, J. H.: Global Evaluation of Radiosonde Water Vapor Systematic Biases using GPS Radio Occultation from COSMIC and ECMWF Analysis, *Remote Sens.*, 2(5), 1320–1330, doi:10.3390/rs2051320, 2010.

Holton, J. R., Haynes, P. H., McIntyre, M. E., Douglass, A. R., Rood, R. B., and Pfister, L.: Stratosphere-troposphere exchange, *Review of Geophysics*, 35, 403–439, doi:10.1029/95RG02097, 1995.

IPCC: Summary for Policymakers, in: *Climate Change 2007: The Physical Science Basis. Contribution of Working Group I to the Fifth Assessment Report of the Intergovernmental Panel on Climate Change*, edited

995 by Solomon, S., Qin, D., Manning, M., Chen, Z., Marquis, M., Averyt, K., M. Tignor, and Miller, H., Cambridge University Press, Cambridge, United Kingdom and New York, USA, 2007.

IPCC: Summary for Policymakers, in: Climate Change 2013: The Physical Science Basis. Contribution of Working Group I to the Fifth Assessment Report of the Intergovernmental Panel on Climate Change, edited by Stocker, T. F., Qin, D., Plattner, G. K., Tignor, M., Allen, S. K., Boschung, J., Nauels, A., Xia, Y., Bex, 1000 V., and Midgley, P., Cambridge University Press, Cambridge, United Kingdom and New York, USA, 2013.

Karl, T. R., Hassol, S. J., Miller, C. D., and (eds), W. L. M.: Temperature Trends in the Lower Atmosphere: Steps for Understanding and Reconciling Differences, Tech. rep., U.S. Climate Change Science Program, Washington, DC, 2006.

Kendall, M. G.: Rank correlation methods, *Journal of the American Statistical Association*, 63, 1379–1389, 1005 doi:10.1080/01621459.1968.10480934, 1962.

Khandu, Awange, J. L., Wickert, J., Schmidt, T., Sharifi, M. A., Heck, B., and Fleming, K.: GNSS remote sensing of the Australian tropopause, *Climate Change*, 105, 597–618, doi:10.1007/s10584-010-9894-6, 2011.

Kripalani, R. H., , Oh, J. H., , Kulkarni, A., , Sabade, S. S., and Chaudhari, H. S.: South Asian summer monsoon precipitation variability: Coupled climate model simulations and projections under IPCC AR4, *Theoretical and Applied Climatology*, 90, 133–159, doi:10.1007/s00704-006-0282-0, 2007. 1010

Krishnamurti, T. N., Stefanova, L., and Misra, V.: Monsoons, in: *Tropical Meteorology: An Introduction*, p. 423, Springer Berlin Heidelberg, 2013.

Kulkarni, J. R. and Verma, R. K.: On the spatio-temporal variations of the tropopause height over India and Indian summer monsoon activity, *Advances in Atmospheric Sciences*, 10, 481–488, doi:10.1007/BF02656973, 1015 1993.

Kumar, G., Madan, R., Saikrishnan, K., Kundu, S. K., and Jain, P. K.: Technical and operational characteristics of GPS sounding system in the upper air network of IMD, *Mausam*, 62, 403–416, available at: metnet.imd.gov.in/mausamdocs/16632_F.pdf, 2011.

Kursinski, E. R., Hajj, G. A., Schofield, J. T., Linfield, R. P., and Hardy, K. R.: Observing Earth’s atmosphere with radio occultation measurements using the Global Positioning System, *Journal of Geophysical Research*, 1020 102, 23 429—23 465, doi:10.1029/97JD01569, 1997.

Lau, W. K. M., Kim, K. M., Hsu, C. N., and Holben, B. N.: Possible influences of air pollution, dust- and sandstorms on the Indian monsoon, *Bulletin - World Meteorological Organization*, 58, 22–30, 2009.

Lee, I. T., Matsuo, T., Richmon, A. D., Liu, J. Y., Wang, W., Lin, C. H., Anderson, J. L., and Chen, M. Q.: 1025 Assimilation of FORMOSAT-3/COSMIC electron density profiles into a coupled thermosphere/ionosphere model using ensemble Kalman filtering, *Journal of Geophysical Research*, 117, doi:10.1029/2012JA017700, 2012.

Lewis, H. W.: A robust method for tropopause altitude identification using GPS radio occultation data, *Geophysical Research Letters*, 36, doi:10.1029/2009GL039231, 2009.

1030 Liang, C. K., Eldering, A., Gettelman, A., Tian, B., Wong, S., Fetzer, E. J., and Liou, K. N.: Record of tropical interannual variability of temperature and water vapor from a combined AIRS-MLS data set, *Journal of Geophysical Research*, 116, doi:10.1029/2010JD014841, 2011.

Lorenz, E. N.: Empirical Orthogonal Functions and Statistical Weather Prediction, Statistical Forecasting Project Scientific Report No. 1, Air Force Research Laboratories, Office of Aerospace Research, USAF, Bedford,

- ford, MA, USA, available at: http://eaps4.mit.edu/research/Lorenz/Empirical_Orthogonal_Functions_1956.pdf, 1956.
- Lott, F. C., Stott, P. A., Mitchell, D. M., Christidis, N., Gillett, N. P., Haimberger, L., Perlwitz, J., and Thorne, P. W.: Models versus radiosondes in the free atmosphere: A new detection and attribution analysis of temperature, *Journal of Geophysical Research*, 118, doi:10.1002/jgrd.50255, 2013.
- Mann, H. B.: Nonparametric Tests Against Trend, *Econometrica*, 13, 245–259, 1945.
- Mehta, S. K., Ratnam, M. V., and Murthy, B. V. K.: Variability of the tropical tropopause over Indian monsoon region, *Journal of Geophysical Research*, 115, doi:10.1029/2009JD012655, 2010.
- Melbourne, W. G., Davis, E. S., Duncan, C. B., Hajj, G. A., Hardy, K. R., Kursinski, E. R., Meehan, T. K., Young, L. E., and Yunck, T. P.: The application of spaceborne GPS to atmospheric limb sounding and global change monitoring, Tech. Rep. JPL-PUBL-94-18, Jet Propulsion Laboratory, California Institute of Technology, Pasadena, CA, United States, 1994.
- Mirza, M. M. Q., Warrick, R., Ericksen, N., and Kenny, G.: Trends and persistence in precipitation in the Ganges, Brahmaputra and Meghna river basins, *Hydrological Sciences*, 43, doi:10.1080/02626669809492182, 1998.
- Pan, L. L., Randel, W. J., Gary, B. L., Mahoney, M. J., and Hints, E. J.: Definitions and sharpness of the extratropical tropopause: A trace gas perspective, *Review of Geophysics*, 109, doi:10.1029/2004JD004982, 2004.
- Poli, P., Healy, S. B., Rabier, F., and Pailleux, J.: Preliminary assessment of the scalability of GPS radio occultations impact in numerical weather prediction, *Geophysical Research Letters*, 35, doi:10.1029/2008GL035873, 2008.
- Poli, P., Healy, S. B., and Dee, D. P.: Assimilation of Global Positioning System radio occultation data in the ECMWF ERA–Interim reanalysis, *Quarterly Journal of the Royal Meteorological Society*, 136, doi:10.1002/qj.722, 2010.
- Preisendorfer, R. W.: Principal component analysis in meteorology and oceanography, Elsevier, 1988.
- PSAS: A Quick Derivation relating altitude to air pressure, Portland State Aerospace Society, US, http://psas.pdx.edu/RocketScience/PressureAltitude_Derived.pdf, 2004.
- Randel, W. J., Wu, F., and Gaffen, D. J.: Interannual variability of the tropical tropopause derived from radiosonde data and NCEP reanalyses, *Journal of Geophysical Research*, 105, 15 509—15 523, doi:10.1029/2000JD900155, 2000.
- Reid, G. C. and Gage, K. S.: Interannual variations in the height of the tropical tropopause, *Journal of Geophysical Research*, 90, 5629–5635, doi:10.1029/JD090iD03p05629, 1985.
- Resmi, E., Mohanakumar, K., and Appu, K.: Effect of polar sudden stratospheric warming on the tropical stratosphere and troposphere and its surface signatures over the Indian region, *Journal of Atmospheric and Solar-Terrestrial Physics*, 105–106, 15–29, doi:10.1016/j.jastp.2013.07.003, 2013.
- Rienecker, M. M., Suarez, M. J., Todling, R., Bacmeister, J., Takacs, L., Liu, H. C., Gu, W., Sienkiewicz, M., Koster, R. D., Gelaro, R., Stajner, I., and Nielsen, J. E.: The GEOS-5 Data Assimilation System—Documentation of versions 5.0.1, 5.1.0, and 5.2.0, NASA Technical Report Series on Global Modeling and Data Assimilation Vol. 27, NASA/TM–2008–104606, NASA Center for Aerospace Information, Maryland, US, 2008.

- 1075 Rienecker, M. M., Suarez, M. J., Gelaro, R., Todling, R., Bacmeister, J., Liu, E., Bosilovich, M. G., Schubert, S. D., Takacs, L., Kim, G. K., Bloom, S., Chen, J., Collins, D., Conaty, A., da Silva, A., Gu, W., Joiner, J., Koster, R. D., Lucchesi, R., Molod, A., Owens, T., Pawson, S., Pegion, P., Redder, C. R., Reichle, R., Robertson, F. R., Ruddick, A. G., Sienkiewicz, M., and Woollen, J.: MERRA: NASA's Modern-Era Retrospective Analysis for Research and Applications, *J. Climate*, 24, 3624–3648, doi:10.1175/JCLI-D-11-00015.1, 2011.
- 1080 Rocken, C., Anthes, R., Exner, M., Hunt, D., Sokolovskiy, S., Ware, R., Gorbunov, M., Schreiner, W., Feng, D., Herman, B., Kuo, Y.-H., and Zou, X.: Analysis and validation of GPS/MET data in the neutral atmosphere, *Journal of Geophysical Research*, 102, 29 849—29 866, doi:10.1029/97JD02400, 1997.
- Saji, N. H., Goswami, B. N., Vinayachandran, P. N., and Yamagata, T.: A dipole mode in the tropical Indian Ocean, *Nature*, 401, 360–363, 1999.
- 1085 Santer, B. D., Wehner, M. F., Wigley, T. M. L., R., Meehl, G. A., Taylor, K. E., Ammann, C., Arblaster, J., Washington, W. M., Boyle, J. S., and Brüggemann, W.: Contributions of Anthropogenic and Natural Forcing to Recent Tropopause Height Changes, *Current Science*, 301, 479–483, doi:10.1126/science.1084123, 2003a.
- Santer, B. D., Sausen, Wigley, T. M. L., Boyle, J. S., andC. Doutriaux, K. A., Hansen, J. E., Meehl, G. A.,
- 1090 Roeckner, E., Ruedy, R., Schmidt, G., and Taylor, K. E.: Behavior of tropopause height and atmospheric temperature in models, reanalyses, and observations: Decadal changes, *Journal of Geophysical Research*, 108, 4ACL 1–1–ACL 1–22, doi:10.1029/2002JD00225, 2003b.
- Santer, B. D., Wigley, T. M. L., Mears, C., Wentz, F. J., Klein, S. A., Seidel, D. J., Taylor, K. E., Thorne, P. W., Wehner, M. F., Gleckler, P. J., Boyle, J. S., Collins, W. D., Dixon, K. W., Doutriaux, C., Free, M.,
- 1095 Fu, Q., Hansen, J. E., Jones, G. S., Ruedy, R., Karl, T. R., Lanzante, J. R., Meehl, G. A., Ramaswamy, V., Russell, G., and Schmidt, G. A.: Amplification of Surface Temperature Trends and Variability in the Tropical Atmosphere, *Science*, 309, 1551–1556, doi:10.1126/science.1114867, 2005.
- Santer, B. D., Thorne, P. W., Haimberger, L., Taylor, K. E., Wigley, T. M. L., Lanzante, J. R., Solomon, S., Free, M., Gleckler, P. J., Jones, P. D., Karl, T. R., Klein, S. A., Mears, C., Nychka, D., Schmidt, G. A., Sherwood,
- 1100 S. C., and Wentz, F. J.: Consistency of modelled and observed temperature trends in the tropical troposphere, *International Journal of Climatology*, 13, 1703–1722, doi:doi:10.1002/joc.1756, 2008.
- Sausen, R. and Santer, B. D.: Use of changes in tropopause height to detect human influences on climate, *Meteorologische Zeitschrift*, 3, 131–136, doi:10.1127/0941-2948/2003/0012-0131, 2003.
- Schmidt, T., Wickert, J., Beyerle, G., and Heise, S.: Global tropopause height trends estimated from GPS radio
- 1105 occultation data, *Geophysical Research Letters*, 35, doi:10.1029/2008GL034012, 2008.
- Schmidt, T., Wickert, J., and Haser, A.: Variability of the upper troposphere and lower stratosphere observed with GPS radio occultation bending angles and temperatures, *Advances in Space Research*, 46, 150–161, doi:10.1016/j.asr.2010.01.021, 2010.
- Seidel, D. J. and Randel, W. J.: Variability and trends in the global tropopause estimated from radiosonde data,
- 1110 *Journal of Geophysical Research*, 111, doi:10.1029/2006JD007363, 2006.
- Seidel, D. J., Ross, R. J., Angell, J. K., and Reid, G. C.: Climatological characteristics of the tropical tropopause as revealed by radiosondes, *Journal of Geophysical Research*, 106, doi:10.1029/2000JD900837, 2001.
- Seidel, D. J., Gillett, N. P., Lanzante, J. R., Shine, K. P., and Thorne, P. W.: Stratospheric temperature trends: our evolving understanding, *WIREs Climate Change*, 2, 592–616, doi:10.1002/wcc.125, 2011.

- 1115 Sen, P. K.: Estimates of the Regression Coefficient Based on Kendall's Tau, *Journal of the American Statistical Association*, 63, 1379–1389, doi:10.1080/01621459.1968.10480934, 1968.
- Sridharan, S., Raghunath, K., Sathishkumar, S., and Nath, D.: Mie lidar and radiosonde observations at Gadanki (13.5°N, 79.2°E) during sudden stratospheric warming of 2009, *Journal of Atmospheric and Solar-Terrestrial Physics*, 73, 544–550, doi:10.1016/j.jastp.2010.11.016, 2011.
- 1120 Steiner, A. K., Lackner, B. C., Ladstädter, F., Scherllin-Pirscher, B., Foelsche, U., and Kirchengast, G.: GPS radio occultation for climate monitoring and change detection, *Radio Science*, 46, doi:10.1029/2010RS004614, 2011.
- Steiner, A. K., Hunt, D., Ho, S.-P., Kirchengast, G., Mannucci, A. J., Scherllin-Pirscher, B., Gleisner, H., von Engeln, A., Schmidt, T., Ao, C., Leroy, S. S., Kursinski, E. R., Foelsche, U., Gorbunov, M., Heise, S., Kuo, Y.-H., Lauritsen, K. B., Marquardt, C., Rocken, C., Schreiner, W., Sokolovskiy, S., Syndergaard, S., and Wickert, J.: Quantification of structural uncertainty in climate data records from GPS radio occultation, *Atmos. Chem. Phys.*, 13, 1469–1484, doi:10.5194/acp-13-1469-2013, 2013.
- 1125 Sun, B., Reale, A., J., D., and Hunt, D. C.: Comparing radiosonde and COSMIC atmospheric profile data to quantify differences among radiosonde types and the effects of imperfect collocation on comparison statistics, *Journal of Geophysical Research*, 115, doi:10.1029/2010JD014457, 2010.
- 1130 Thorne, P. W., Brohan, P., Titchner, H. A., McCarthy, M. P., Sherwood, S. C., Peterson, T. C., Haimberger, L., Parker, D. E., Tett, S. F. B., Santer, B. D., Fereday, D. R., , and Kennedy, J. J.: A quantification of uncertainties in historical tropical tropospheric temperature trends from radiosondes, *Journal of Geophysical Research*, 116, doi:10.1029/2010JD015487, 2013.
- 1135 Trenberth, K. E.: Recent Observed Interdecadal Climate Changes in the Northern Hemisphere, *Bull. Amer. Meteor. Soc.*, 71, 988–993, doi:10.1175/1520-0477(1990)071<0988:ROICCI>2.0.CO;2, 1990.
- Ware, R., Rocken, C., Solheim, F., Exner, M., Schreiner, W., Anthes, R., Feng, D., Herman, B., Gorbunov, M., Sokolovskiy, S., Hardy, K., Kuo, Y., Zou, X., Trenberth, K., Meehan, T., Melbourne, W., and Businger, S.: GPS Sounding of the Atmosphere from Low Earth Orbit: Preliminary Results, *Bull. Amer. Meteor. Soc.*, 77, 19–40, doi:10.1175/1520-0477(1996)077<0019:GSOTAF>2.0.CO;2, 1996.
- 1140 Wickert, J., Reigber, C., Beyerle, G., König, R., Marquardt, C., Schmidt, T., Grunwaldt, L., Galas, R., Meehan, T. K., Melbourne, W. G., and Hocke, K.: Atmosphere sounding by GPS radio occultation: First results from CHAMP, *Geophysical Research Letters*, 28, 29 849–29 866, doi:10.1029/2001GL013117, 2001.
- Wickert, J., Michalak, G., Schmidt, T., Beyerle, G., Cheng, C. Z., Healy, S. B., Heise, S., Huang, C. Y., Jakowski, N., Kohler, W., Mayer, C., Offiler, D., Ozawa, E., Pavelyev, A. G., Rothacher, M., Tapley, B., and Arras, C.: GPS Radio Occultation: Results from CHAMP, GRACE and FORMOSAT-3/COSMIC, *Terr. Atmos. Ocean. Sci.*, 20, 35–50, doi:10.3319/TAO.2007.12.26.01(F3C), 2009.
- 1145 Wilcox, L. J., Hoskins, B. J., and Shine, K. P.: A global blended tropopause based on ERA data. Part II: Trends and tropical broadening, *Journal of Geophysical Research*, 138, 576–584, doi:10.1002/qj.910, 2011.
- 1150 WMO: Meteorology - A three-dimensional science: Second session of the commission for aerology, *WMO Bulletin*, IV, 134–138, 1957.
- Zhang, M. L., Liu, L., Wan, W., and B. . N.: An update global model of hmF2 from values estimated from ionosonde and COSMIC/FORMOSAT-3 radio occultation, *Advances in Space Research*, 53, 395–402, doi:10.1016/j.asr.2013.11.053, 2014.

- 1155 Zhang, X. and Srinivasan, R.: GIS-based spatial precipitation estimation: a comparison of geostatistical approaches, *Journal of the American Water Resources Association*, 45, 894—906, doi:10.1111/j.1752-1688.2009.00335.x, 2009.

Table 1. Correlation coefficients between ocean-atmospheric climate indices and temperature anomalies at 200 hPa, 100 hPa, 70 hPa, and 50 hPa for the period August 2006 to December 2013.

Pressure Levels	ENSO		IOD		QBO	
	Correlation	Lag (months)	Correlation	Lag (months)	Correlation	Lag (months)
200 hPa	-0.70	0	-0.42	0	0.39	26
100 hPa	0.82	1	0.27	2	0.47	27
70 hPa	0.40	3	-0.35	-4	-0.45	25
50 hPa	0.27	1	0.34	2	0.53	12

Table 2. Trends in temperature ($^{\circ}\text{C}$) at 200 hPa, 100 hPa, 70 hPa, and 50 hPa for the period August 2006 to December 2013.

Pressure Levels	COSMIC	MERRA	ERA-Interim
200 hPa	0.02 ± 0.02	0.03 ± 0.03	0.03 ± 0.05
100 hPa	-0.04 ± 0.05	0.00 ± 0.00	-0.02 ± 0.04
70 hPa	-0.07 ± 0.05	-0.04 ± 0.05	-0.05 ± 0.05
50 hPa	-0.02 ± 0.04	-0.01 ± 0.01	-0.01 ± 0.02

Table 3. Trends in tropopause parameters (temperature and height) based on the area-averaged time-series anomalies derived from COSMIC RO and MERRA. Data span between August 2006 and December 2013.

Data	Temperature ($^{\circ}\text{C}$)	Height (meters)
COSMIC RO	-0.039 ± 0.05	6.01 ± 5.02
MERRA	-0.005 ± 0.03	17.00 ± 10.20

Table 4. Correlation coefficients between tropopause parameters (temperature and height) derived from COSMIC RO and MERRA and ocean-atmospheric indices for the period August 2006 to December 2013.

Data	COSMIC RO		MERRA	
	Temperature	Height	Temperature	Height
Nino3.4 & PC 1	0.77	-0.74	0.78	-0.75
IOD & PC 1	0.35	0.37	0.35	0.38
QBO & PC 2	0.36	0.36	0.53	0.54

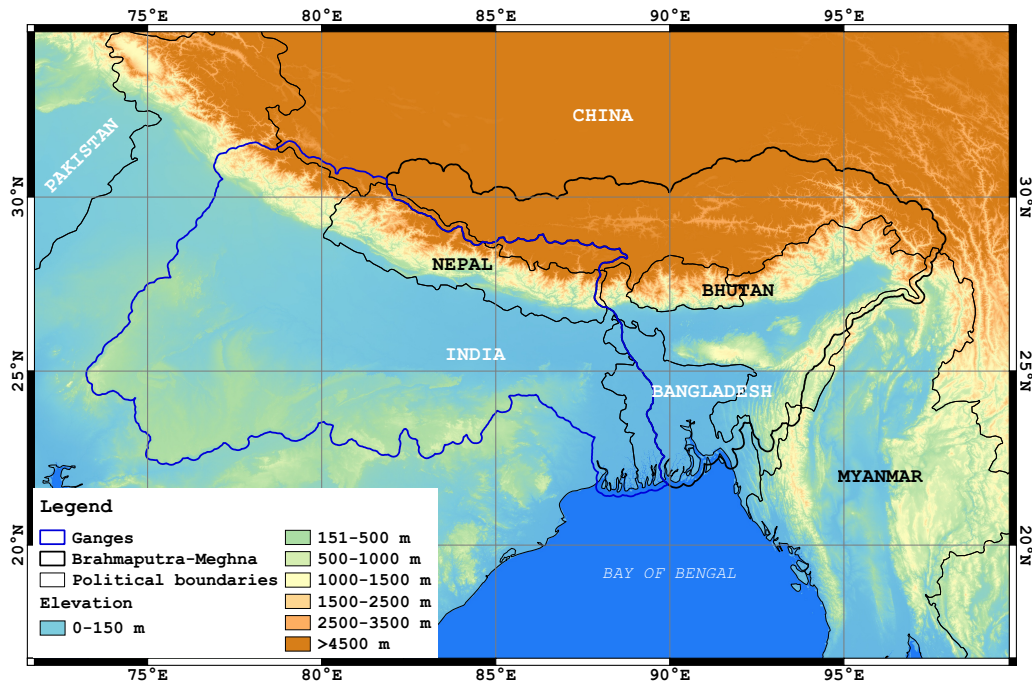


Figure 1. Elevation of the Ganges-Brahmaputra-Meghna Basin in South Asia. The digital elevation model is derived from the Shuttle Radar Topography mission (SRTM, <http://srtm.csi.cgiar.org>). The locations of the existing radiosonde stations are shown in circles (black).

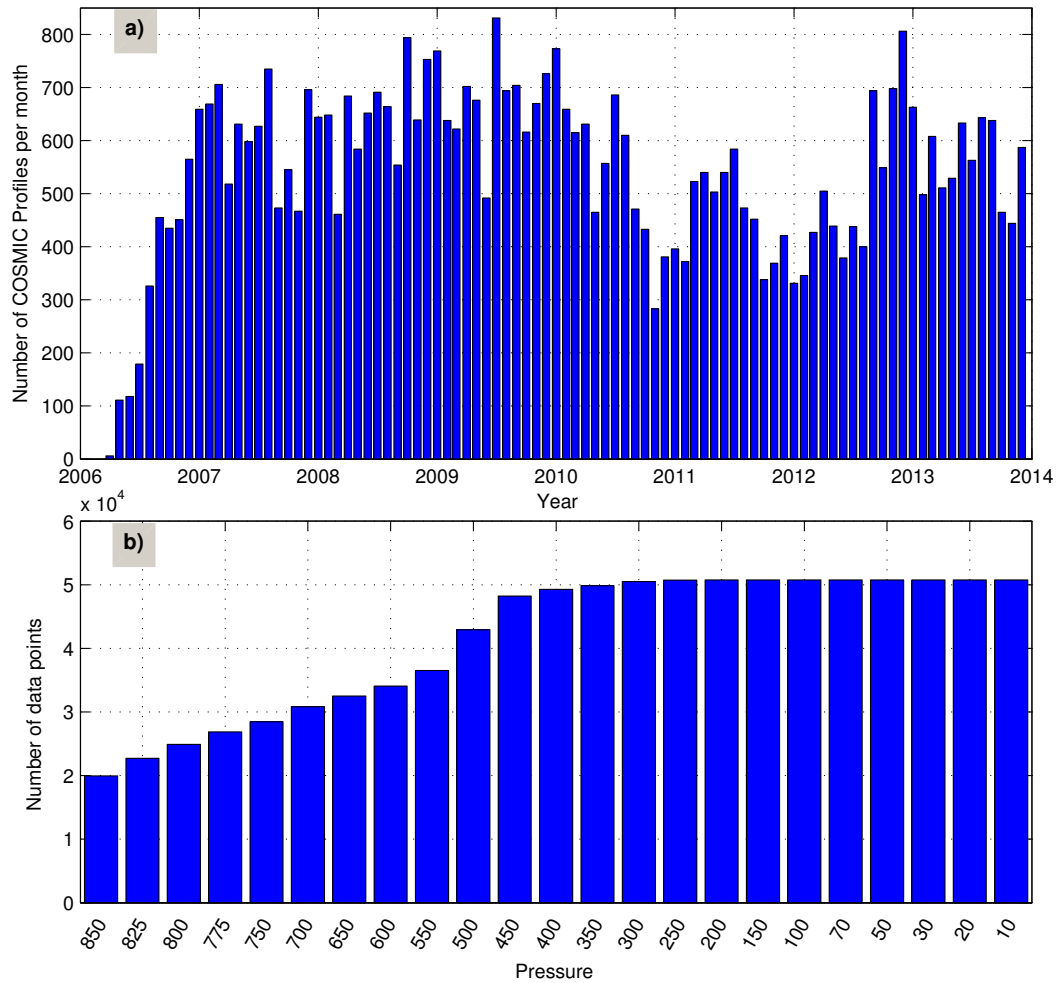


Figure 2. a) **Total number of monthly** COSMIC RO profiles reported in and around the GBM basin between April 2006 and December 2013, and b) the corresponding number of data points at each pressure levels 850-30 hPa (1.5-24.0 km).

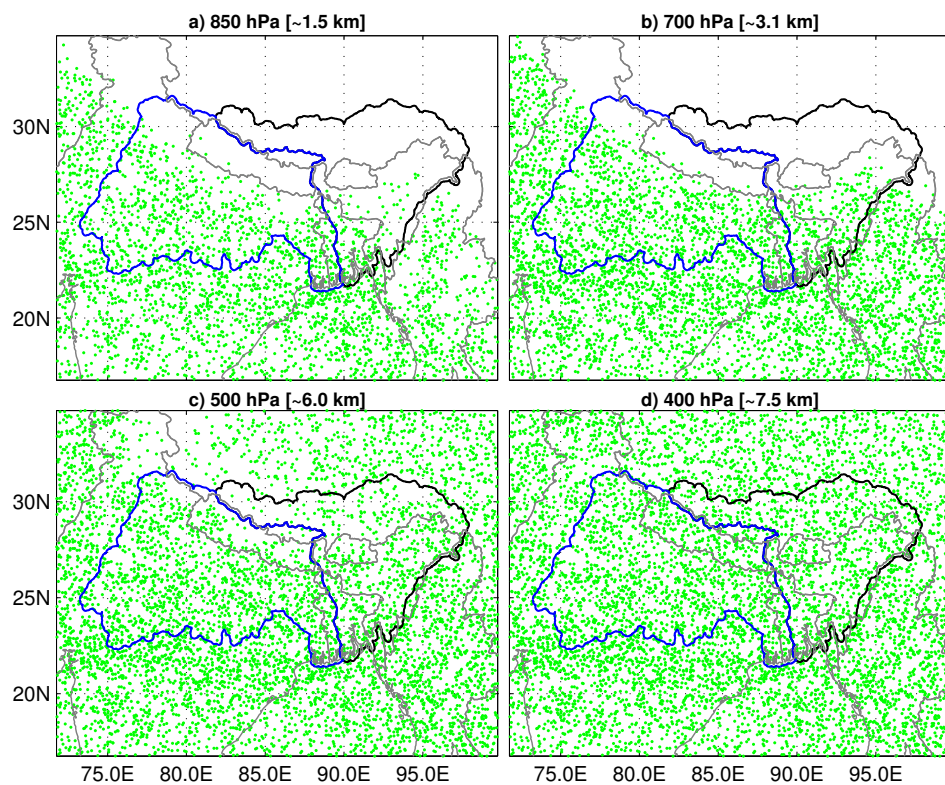


Figure 3. a) Spatial distribution of COSMIC data points in the lower troposphere for the year 2012: a) 850 hPa (~1.5 km), b) 700 hPa (~3.1 km), c) 500 hPa (~5.8 km), and d) 400h Pa (~7.5 km).

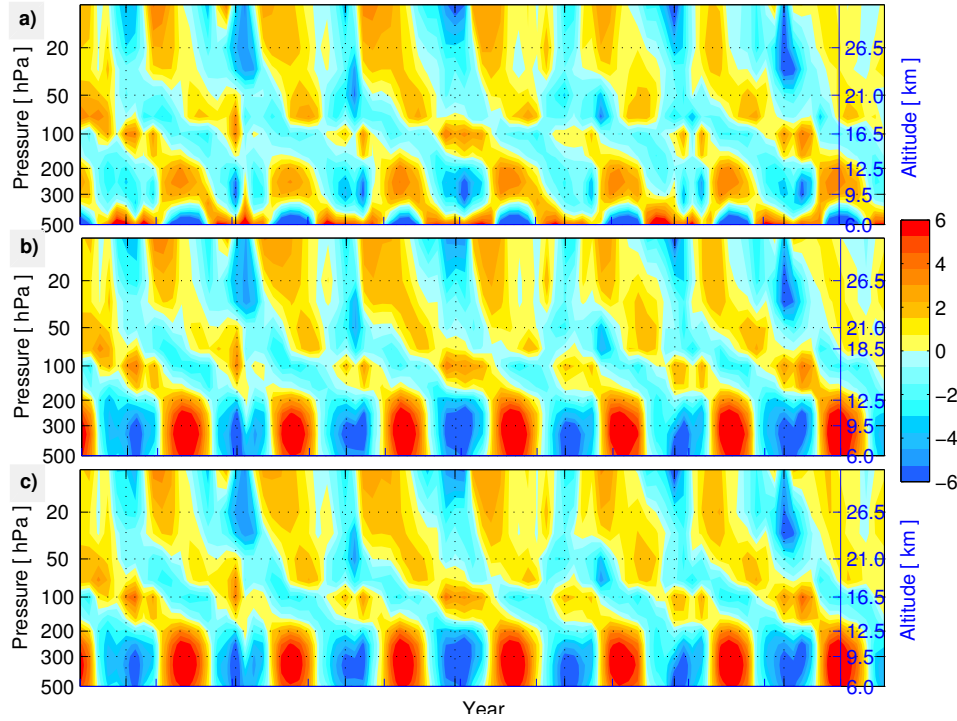


Figure 4. Temporal evolution of temperature($^{\circ}\text{C}$) with the time mean removed at each pressure level (500-10 hPa) based on (a) COSMIC RO, (b) MERRA, and (c) ERA-Interim. Data spans between August 2006 and December 2013 and contains area-weighted average over the region (16°N - 35°N , 71°E - 100°E) covering the GBM basin. Mean air temperature between 500–30 hPa (or 6.0–24.5 km) for the period August 2006–December 2013. (a) COSMIC wet profiles, (b) MERRA re-analysis product, and (c) Mean temperature difference between MERRA and COSMIC data.

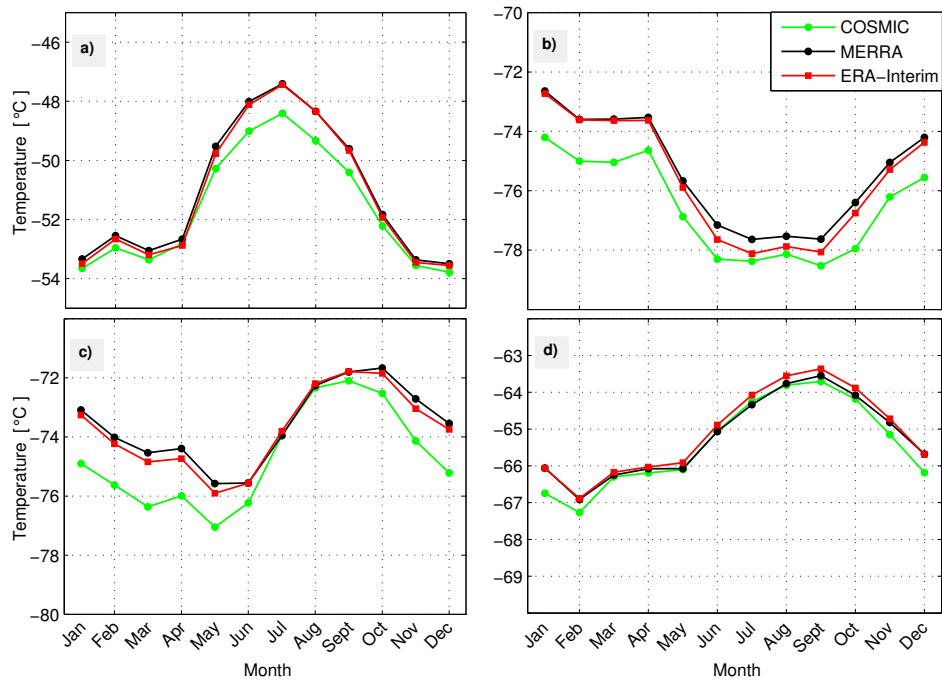


Figure 5. Seasonal cycle of temperature(°C) at (a) 200 hPa, (b) 100 hPa, (c) 70 hPa, and (d) 50 hPa from August 2006 to December 2013 based on COSMIC RO, MERRA, and ERA-Interim averaged over the GBM basin.

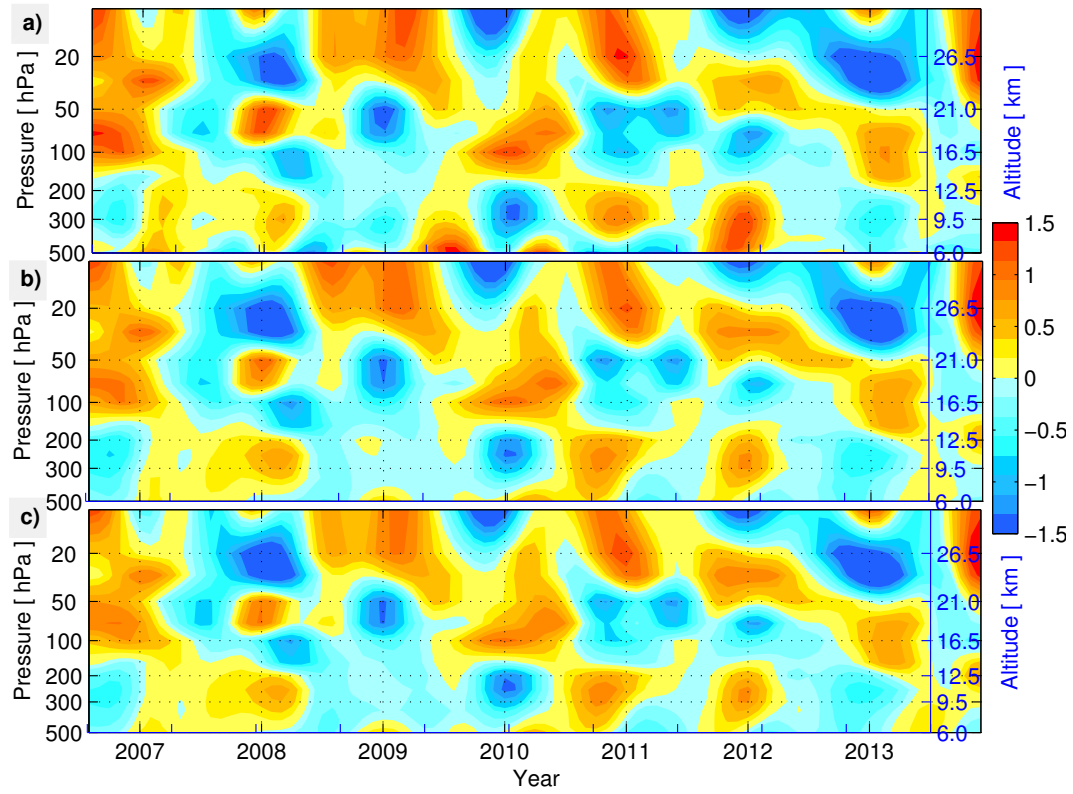


Figure 6. Interannual variability of temperature ($^{\circ}\text{C}$) in the UTLS region based on (a) COSMIC RO, (b) MERRA, and (c) ERA-Interim from August 2006 to December 2013.

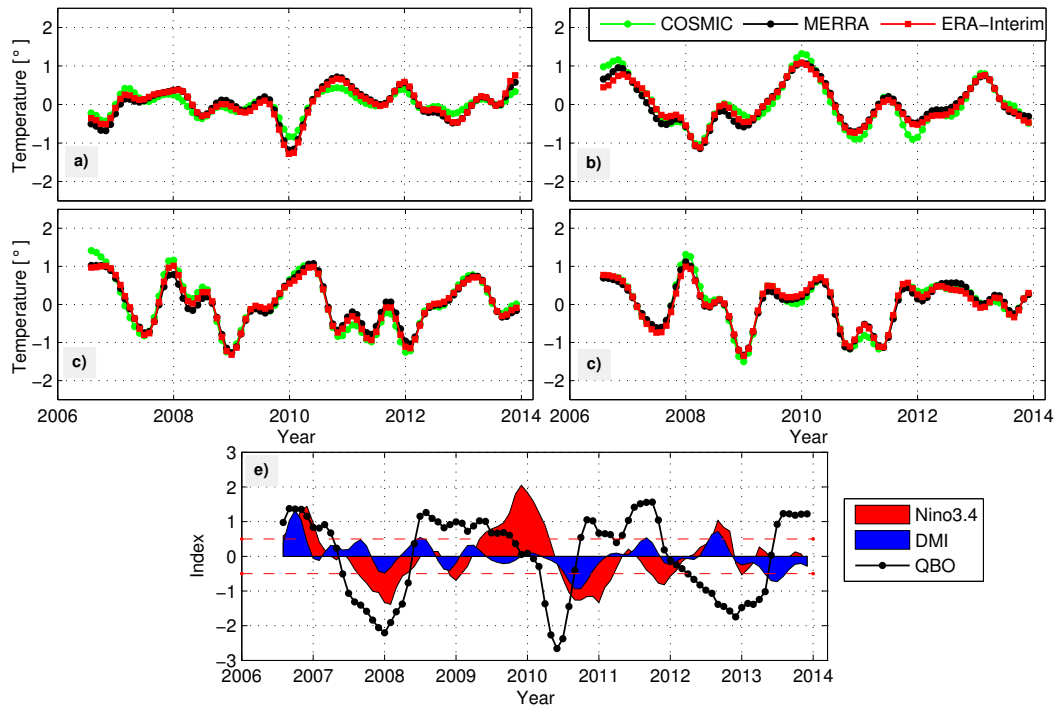


Figure 7. Interannual variability of temperature ($^{\circ}\text{C}$) at (a) 200 hPa, (b) 100 hPa, (c) 70 hPa, and (d) 50 hPa from August 2006 to December 2013 based on COSMIC RO, MERRA, and ERA-Interim. (e) Ocean-atmospheric indices: Niño3.4, DMI, and QBO are also plotted for reference.

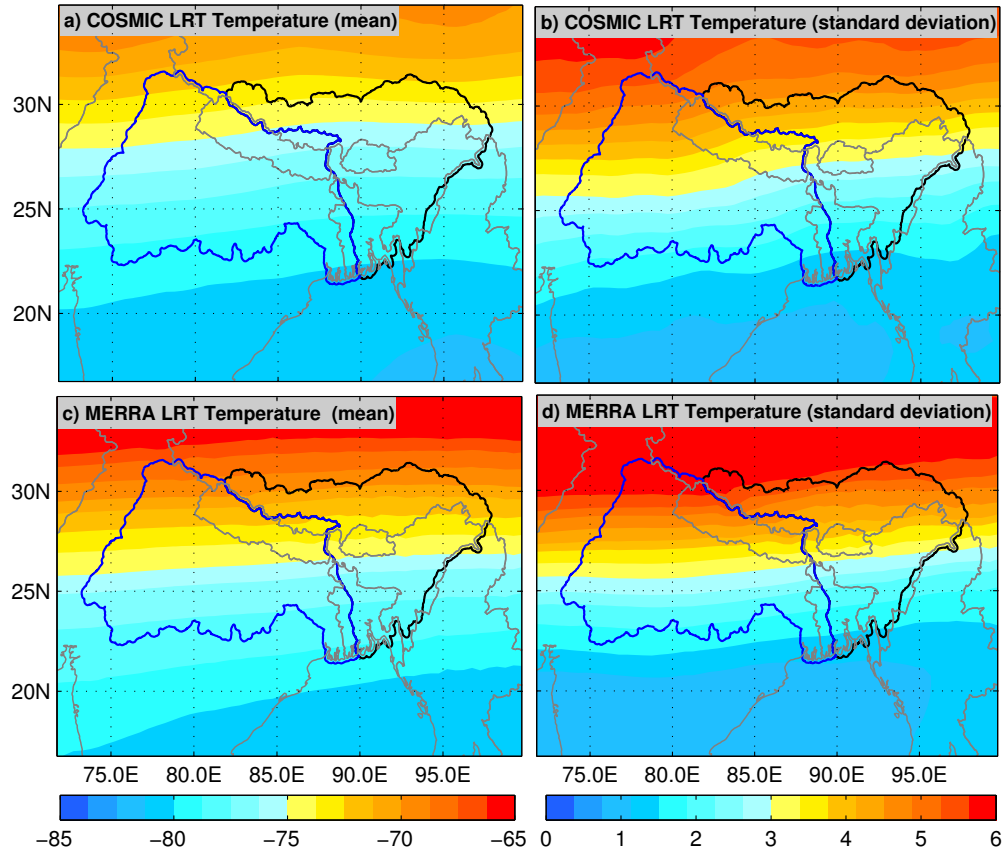


Figure 8. Spatial variation of mean and standard deviation of tropopause temperatures (°C) derived from COSMIC RO and MERRA product based on 89 months from August 2006 to December 2013. (a) Mean and (b) standard deviation of tropopause temperatures (°C) from COSMIC RO, (c) mean and (d) standard deviation of tropopause temperatures (°C) from MERRA product.

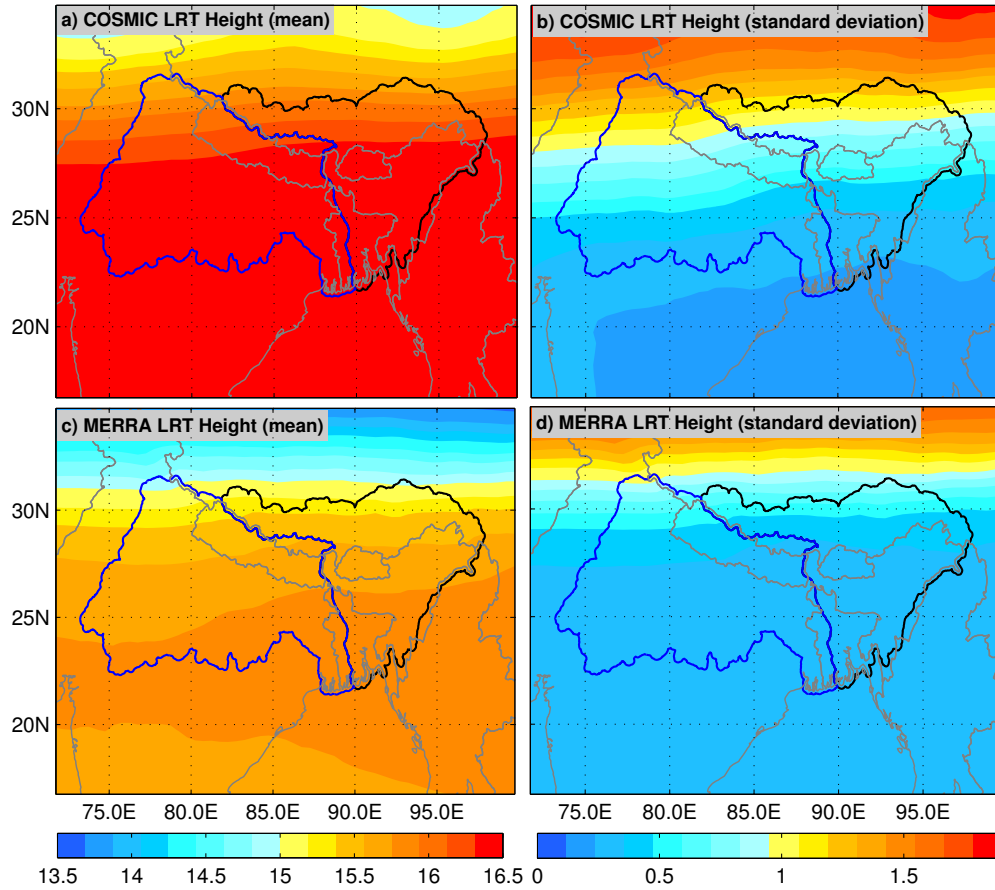


Figure 9. Spatial variation of mean and standard deviation of tropopause heights (km) derived from COSMIC RO and MERRA product based on 89 months from August 2006 to December 2013. (a) Mean and (b) standard deviation of tropopause heights (km) from COSMIC RO, (c) mean and (d) standard deviation of tropopause heights (km) from MERRA product.

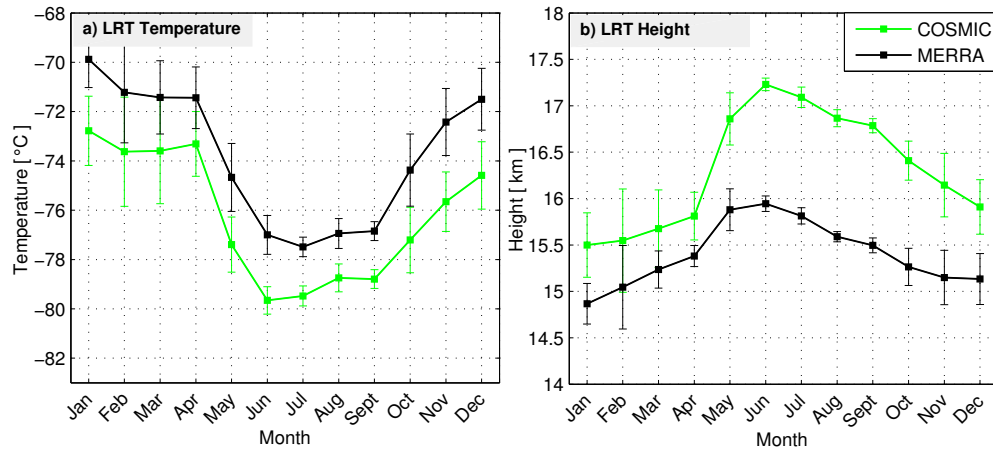


Figure 10. Annual cycle of tropopause over the GBM basin computed from MERRA and COSMIC RO data for the period between August 2006 and December 2013: a) tropopause temperatures, and b) tropopause heights. The seasonal variations correspond reasonably well with Figures 12 and 13 considering that factors impacting the interannual variabilities were effectively removed in Figures 12 and 13 based on the multi-linear regression approach in Equation 4.

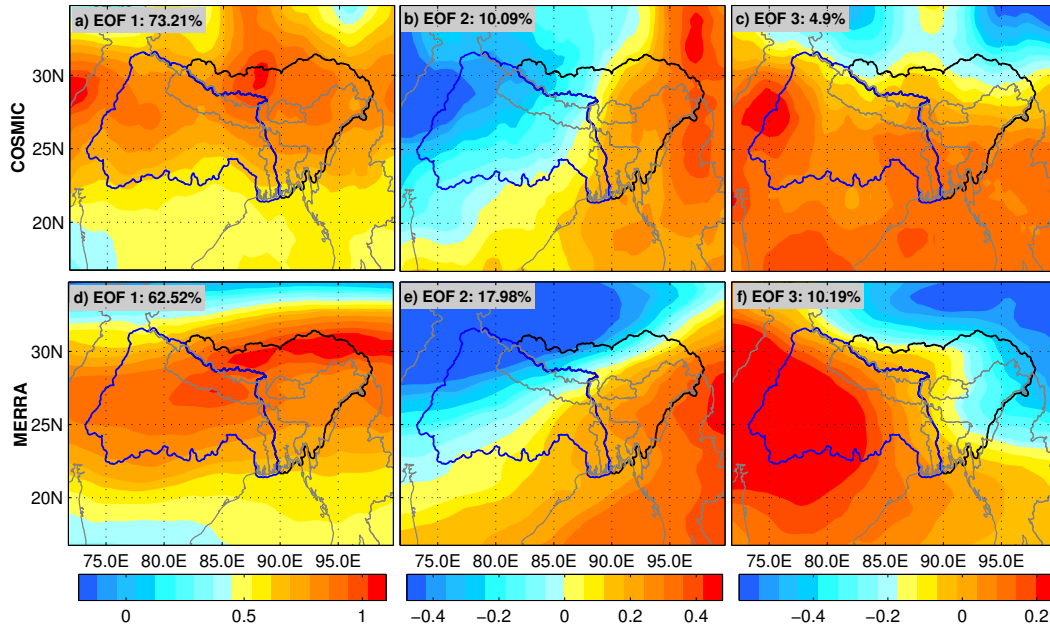


Figure 11. The first three leading EOFs of tropopause temperature (°C) over GBM basin based on MERRA data and COSMIC RO data for the period August 2006 to December 2013, and their relations to major climatic indices in the region.

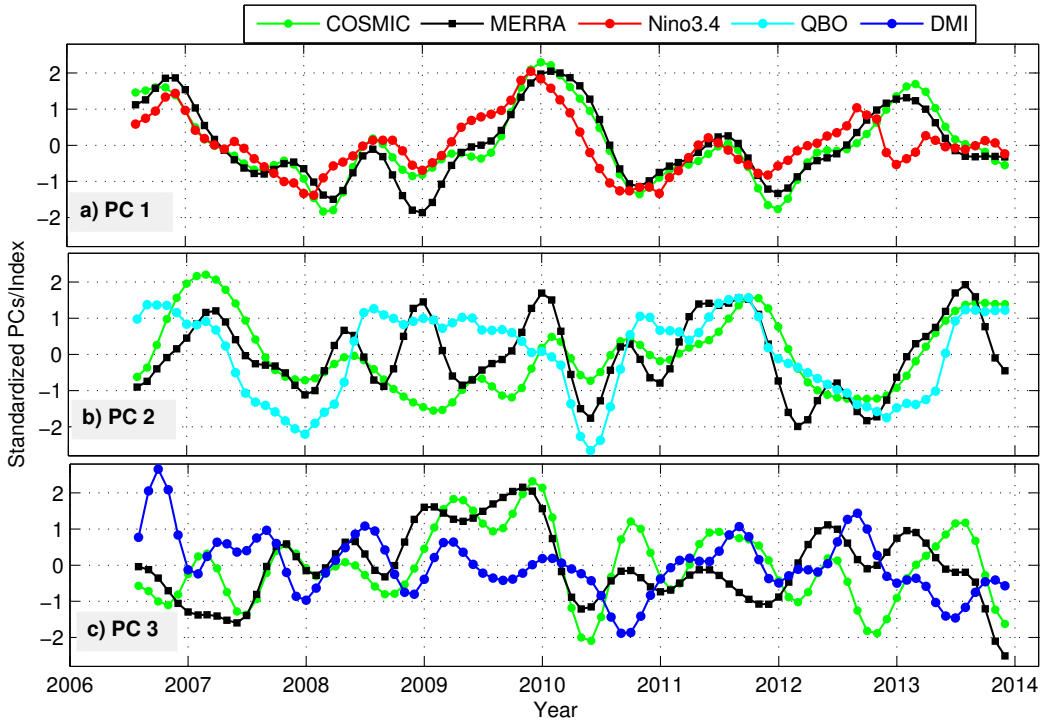


Figure 12. The corresponding PCs (temporal components) based on the three leading orthogonal modes shown in Figure 11. Interannual variability of tropopause temperatures and heights over GBM basin based on MERRA data and COSMIC RO data for the period August 2006 to December 2013, and their relations to major climatic indices in the region.

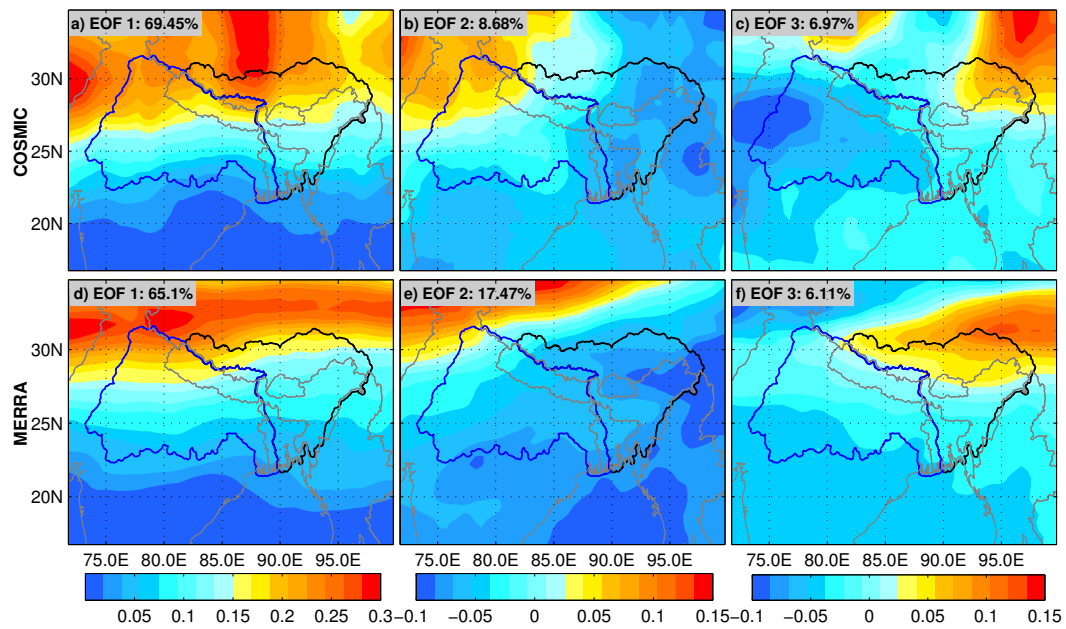


Figure 13. The first three leading EOFs of tropopause height (km) Interannual variability of tropopause temperatures and heights over GBM basin based on MERRA data and COSMIC RO data for the period August 2006 to December 2013, and their relations to major climatic indices in the region.

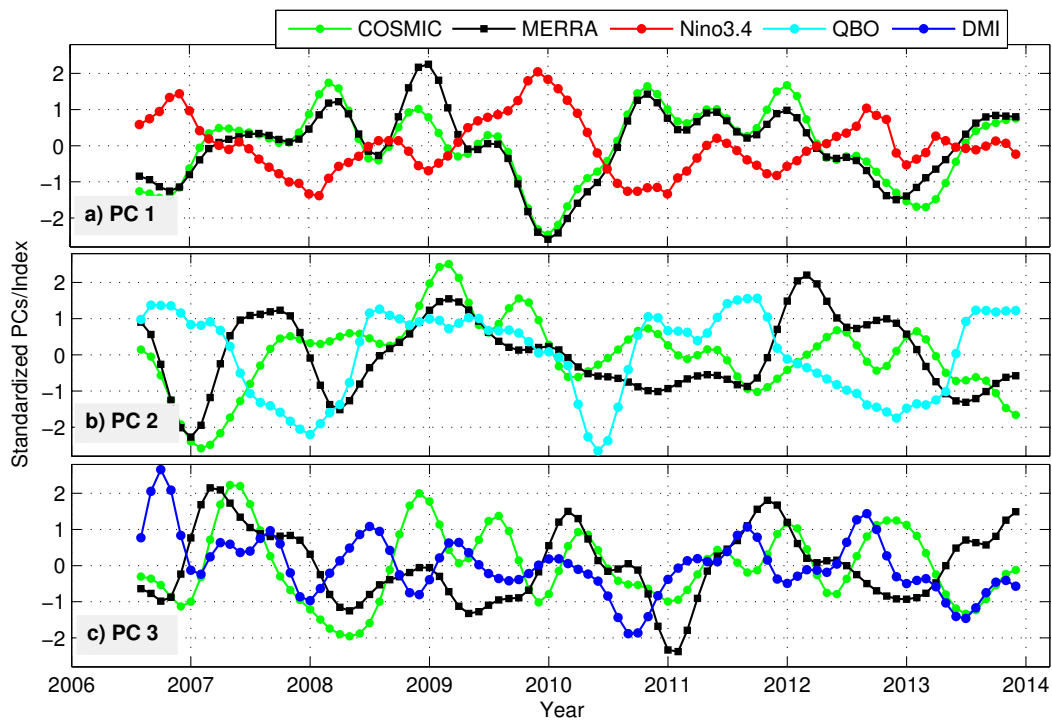


Figure 14. The corresponding PCs (temporal components) based on the three leading orthogonal modes shown in Figure 13. Interannual variability of tropopause temperatures and heights over GBM basin based on MERRA data and COSMIC RO data for the period August 2006 to December 2013, and their relations to major climatic indices in the region.

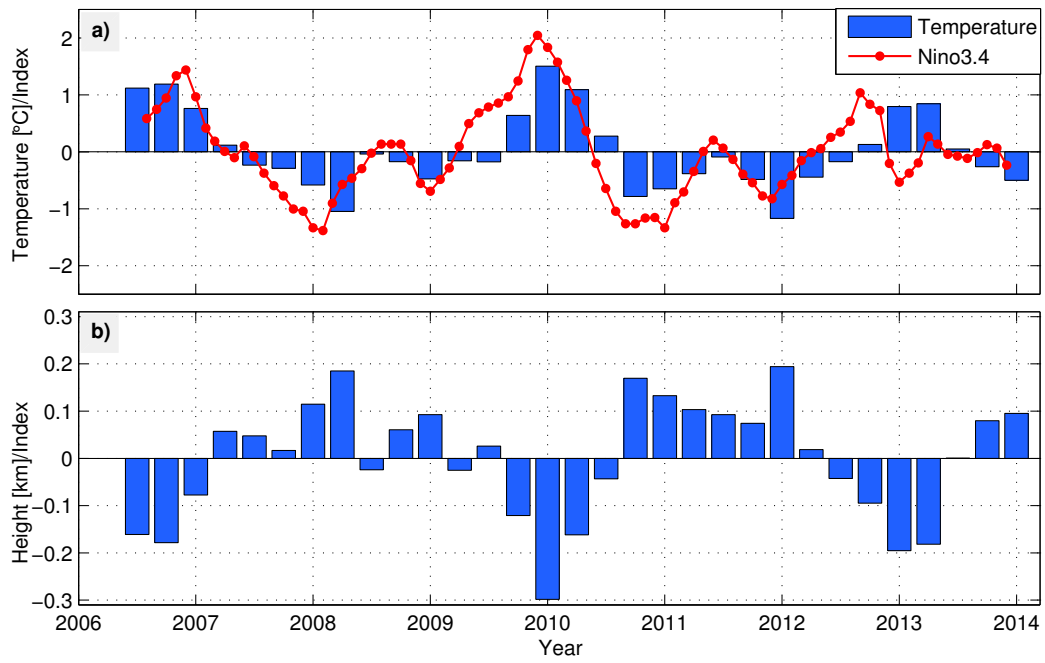


Figure 15. Seasonal mean tropopause temperature and height anomalies due to ENSO mode together with the Niño3.4 index. The area-averaged time series were obtained by multiplying EOF 1 and PC 1, i.e., basically showed the replication of ENSO mode.